The International Journal of Medical Robotics and Computer Assisted Surgery

Development of a flexible parallel wire robot for epicardial interventions

Journal:	*The International Journal of Medical Robotics and Computer Assisted Surgery*
Manuscript ID	RCS-24-0275
Wiley - Manuscript type:	Original Article
Date Submitted by the Author:	10-Jul-2024
Complete List of Authors:	Ladak, Aman; Carnegie Mellon University College of Engineering Bonatti, Johannes O.; University of Pittsburgh Department of Cardiothoracic Surgery Hajjar, Roger J.; Mass General Brigham Inc Shalaby, Alaaeldin A.; University of Pittsburgh Department of Medicine Riviere, Cameron; Carnegie Mellon University Robotics Institute
Primary Area:	Both
Operation Keywords:	
Keywords:	epicardial intervention, beating-heart surgery, subxiphoid access, robotic surgery, gene therapy, cable-driven parallel robots
Specialty Keywords:	
Technology Keywords:	
Anatomy Keywords:	
Abstract:	**Background:** HeartPrinter is a flexible parallel wire robot that adheres to the beating heart with vacuum suction at three bases. An injector head actuated by cables delivers gene therapy injections within the bounds of the bases. To deploy onto the epicardium, an introducer mechanism is required. On the heart, determining the robot's workspace and registering an anatomical model to its pose are required. **Methods:** We present HeartPrinter's components and introducer mechanism, and assess them on an artificial beating heart. We evaluate accuracy for position determination of the bases and registering a three-dimensional heart scan. **Results:** The introducer mechanism successfully positioned HeartPrinter, and the bases adhered to the beating heart. The base positions and registration were determined accurately with errors under 4 mm and 2 mm, respectively. **Conclusions:** The introducer mechanism can deploy HeartPrinter on the epicardium and HeartPrinter's components can operate on the heart. Workspace determination and registration demonstrate feasibility.

Development of a flexible parallel wire robot for epicardial interventions

Authors: Aman Ladak[1], Johannes O. Bonatti[2], Roger J. Hajjar[3], Alaaeldin A. Shalaby[4], and Cameron N. Riviere[5]

Affiliation:

[1]Department of Mechanical Engineering, Carnegie Mellon University, Pittsburgh, Pennsylvania, USA

[2]Department of Cardiothoracic Surgery, University of Pittsburgh, Pittsburgh, Pennsylvania, USA

[3]Gene and Cell Therapy Institute, Mass General Brigham, Boston, Massachusetts, USA

[4]Department of Medicine, University of Pittsburgh, Pittsburgh, Pennsylvania, USA

[5]The Robotics Institute, Carnegie Mellon University, Pittsburgh, Pennsylvania, USA

Corresponding author: Cameron N. Riviere, Ph.D., The Robotics Institute, Carnegie Mellon University, 5000 Forbes Ave, Pittsburgh, Pennsylvania, 15213, USA.

Email: camr@ri.cmu.edu

Phone: +1(412)268-3083

Fax: +1(412)268-7350

submitted to

The International Journal of Medical Robotics and Computer Assisted Surgery

Category: Original article

Word count: 9627

Number of figures: 21

Number of tables: 4

Ethics Statement

Not applicable - case report is not submitted and no participants were involved.

Data Availability

The data that supports the findings of this study are available from the corresponding author upon reasonable request.

Conflict of Interest

C. N. Riviere reports holding equity in HeartLander Surgical, Inc., and is a co-inventor of U.S. patent US10736703B2, held by Carnegie Mellon University. The authors report no other conflicts of interest in this work.

Funding Statement

This research was partially supported by the U.S. National Institutes of Health (grant nos. R01HL078839 and R01HL105911), and Carnegie Mellon University's GSA/Provost GuSH Grant.

Author Contribution Statement

Conceptualization and Design: Aman Ladak

Data Collection: Aman Ladak

Data Analysis: Aman Ladak

Writing – original draft preparation: Aman Ladak

Writing – reviewing: Cameron N. Riviere, Johannes O. Bonatti, Roger J. Hajjar, Alaaeldin A. Shalaby

Writing – editing: Aman Ladak

Clinical Insight: Johannes O. Bonatti, Roger J. Hajjar, Alaaeldin A. Shalaby

Supervision: Cameron N. Riviere

Funding Acquisition: Cameron N. Riviere, Aman Ladak

Final Approval: All authors have read and approved the final version of the manuscript.

Abstract

Background: HeartPrinter is a flexible parallel wire robot that adheres to the beating heart with vacuum suction at three bases. An injector head actuated by cables delivers gene therapy injections within the bounds of the bases. To deploy onto the epicardium, an introducer mechanism is required. On the heart, determining the robot's workspace and registering an anatomical model to its pose are required.

Methods: We present HeartPrinter's components and introducer mechanism, and assess them on an artificial beating heart. We evaluate accuracy for position determination of the bases and registering a three-dimensional heart scan.

Results: The introducer mechanism successfully positioned HeartPrinter, and the bases adhered to the beating heart. The base positions and registration were determined accurately with errors under 4 mm and 2 mm, respectively.

Conclusions: The introducer mechanism can deploy HeartPrinter on the epicardium and HeartPrinter's components can operate on the heart. Workspace determination and registration demonstrate feasibility.

Keywords: epicardial intervention, beating-heart surgery, subxiphoid access, robotic surgery, gene therapy, cable-driven parallel robots

Introduction

Over the years, the field of clinical gene therapy has grown from both a regulatory standpoint and commercially.[1] The progression of cardiac gene therapy has, however, stalled,[2] primarily due to inadequate gene delivery mechanisms to the myocardium.[3,4] While various cardiac gene therapy trials are being undertaken along with advances in identifying signaling pathways and vector creation,[3] the detectable levels of therapeutic expression in myocytes using current delivery methods have not been sufficient for effective heart disease and heart failure treatment.[4]

Gene therapy functions as targeted therapeutic treatment in order to correct mutated genes or specific modifications that are associated with disease prevalence.[4,5] Recombinant adeno-associated virus vectors, which lack viral DNA, are particularly attractive for gene therapy as they can traverse the cell membrane and deliver their DNA cargo into the nucleus of a cell.[6,7] For cardiac gene therapy, since myocytes are primarily non-dividing cells, this makes them ideal targets for adeno-associated virus vectors.[6] An example application of cardiac gene therapy is modulating atrioventricular nodal conduction for rate control by modification of target cells.[8]

Numerous delivery methods have been developed for cardiac gene therapy, such as aortic cross clamping, intravenous injection, and antegrade coronary artery injection.[3] However, such mechanisms have not performed well,[8] demonstrating insufficient levels of transduction efficiency and uniformity.[3] Direct gene injection into the myocardium is one method that has previously shown promise,[4,9] however with current instrumentation, only a small area of the myocardium can be reached.[6] This results in gene expression over a limited region, representing a lack of diffusion of the vector genome into myocytes,[6,9] and therefore no therapeutic response throughout the myocardium.[9] The optimal gene delivery method must ensure the proportion of targeted tissue is reflective of the disease application.[3] In particular, for most arrythmia and heart failure applications, effective direct injection requires numerous small and accurate injections over a large area of the myocardium.[10] As this produces dense and homogenous gene expression at the target site,[11] the morbidity of cardiopulmonary bypass could also be avoided if these injections are delivered while the heart is beating.[12,13]

Cardiac interventions have continued to evolve from standard open procedures, becoming more minimally invasive and thereby decreasing patient recovery times, risk of infection, and scarring.[14,15] With minimally invasive thoracoscopic techniques, however, which utilize rigid tools, the surgeon's workspace is diminished, which restricts the efficacy of gene therapy delivery with direct injection to the myocardium.[6] Alternatively, robotic minimally invasive surgery is a feasible option due to increased access, repeatability, and dexterity.[15,17,18,19] However, for cardiac robotic systems, addressing the heartbeat has presented a challenge,[17,20,21] particularly due to minimal space available within the thorax[22] and arrhythmia which increases the challenge of motion prediction.[23]

A robotic system designed for minimally invasive cardiac gene therapy injections is HeartPrinter,[13] shown in Fig. 1. HeartPrinter is a flexible parallel wire robot that is inserted via a subxiphoid approach to the pericardial space, and deployed on the epicardium using an introducer mechanism.[24] The robot adheres to the beating heart through vacuum pressure at its three suction bases, thereby forming a stable platform that passively compensates the heartbeat and respiratory motion of the heart.[24,25] This eliminates the morbidity associated with arrested heart surgery, such as neurologic dysfunction and damage to major vessels,[22] and removes the need for lung deflation.[24] Within the triangular workspace formed by the suction bases, which spans the region defined by the left ventricle, an injector head can translate along the epicardium via three cables that attach to its sides.[25] Each cable passes from the injector head through a suction base and exits the patient through the subxiphoid access port, and is controlled by an actuator that is housed within the tabletop setup adjacent to the patient, shown in Fig. 2. The actuators control the injector head's position by changing cable lengths between the injector head and the respective suction base.[26,27] This cable-driven design allows HeartPrinter to administer many accurate direct gene injections rapidly over a large region of the beating heart.[27] The region of the epicardium defined by the left ventricle is targeted for injection, as numerous potential gene therapy mechanisms are being investigated to preserve left ventricle function.[28]

As HeartPrinter is a parallel wire robot, also known as a cable-driven parallel robot, its end effector is controlled by flexible cables, which makes it ideal for tasks performed on a large workspace and which

require flexibility.[29] These robots have small inertia and a high payload-to-weight ratio, enabling the end-effector to operate swiftly on its workspace.[29,30] Since HeartPrinter is an under-constrained system with three cables and three degrees of freedom,[27] and the cables that control the end-effector can only exert tensile forces,[31] the system is dependent entirely on its tabletop actuators to maintain tension in the cables that attach to the injector head.[27]

This flexibility of HeartPrinter, however, makes intrapericardial deployment challenging after insertion into the pericardial space,[24] specifically for positioning the suction bases on the epicardium anteriorly, posteriorly, and near the apex of the heart. Moreover, the initial designs of HeartPrinter did not consider compatibility with such a positioning mechanism, and were also relatively large in size, thereby limiting the extent of minimal invasiveness. The surgical workflow, including determination of the workspace and registration of the pose of the robot, along with the analogous software pipeline, had yet to be developed for HeartPrinter.

This paper addresses these needs by presenting significant new development of the HeartPrinter system from a hardware and software standpoint. Firstly, the development of HeartPrinter's components for operating on the epicardium and the tabletop hardware setup are presented. This new design reduces the footprint of the robot and is compatible with the introducer mechanism used to deploy the robot on the heart. Secondly, further development of the introducer mechanism is shown through design, prototyping, and testing, improving upon the concepts presented previously.[24] The mechanism makes use of specialized tools to gain and maintain access in the intrapericardial space, and a steerable mechanism used to guide the suction bases to their respective target regions. Evaluation of the new design of HeartPrinter and introducer mechanism is performed on a rubber beating-heart model using a subxiphoid approach.

Once HeartPrinter is deployed on the heart, a routine is presented for determining the bounds of the robot's workspace, and a method for registering a preoperative anatomical heart model to the pose of the robot. In this work, determination of the robot's workspace and registration of its pose are formulated within the pericardial sac on a static heart without beating and the thorax, building off the most recent study for HeartPrinter performed on a 3D-printed prolate ellipsoid.[26]

Materials and Methods

A. Testing Model Setup

A rubber beating-heart model (Model 1008, The Chamberlain Group, Great Barrington, MA, USA) was used for testing the introducer mechanism with the new design of the robot. The same heart model was used without the beating functionality for evaluating the workspace determination and registration subsystems. When the beating functionality was used, the pulse rate was set to 72 beats per minute[24,32] to mimic that of a live human heart. As seen in Fig. 3A-3B, the heart was positioned anatomically with respect to the thorax (Model 1077, The Chamberlain Group, Great Barrington, MA, USA). The thorax was not used for evaluating the workspace determination and registration subsystems in this study, but was used for evaluating HeartPrinter's components and the introducer mechanism.

In order to more realistically simulate operation on a living patient, a diameter-reducer was added to the subxiphoid access port on the thorax to reduce the diameter of the opening to 20 mm, shown in Fig. 3B. A pericardial sac (Model 1112, The Chamberlain Group, Great Barrington, MA, USA) was fitted over the heart to replicate the pericardium and the target regions for the suction bases on the epicardium were indicated on the pericardial sac with a marker, as shown in Fig. 3C-3D. For some processes, a flashlight was placed within the thorax to increase visibility for imaging. For tests requiring force measurements, a force gauge (Nextech Global Company Limited, Thailand) was used.

B. Hardware Development

i. Robot Components

The prototype of HeartPrinter used in this study is shown in Fig. 4, comprised of the components which will be described in the following sections.

a) Superior Suction Bases

The design of the superior suction bases is shown in Fig. 5, with the posterior suction base shown as an example. HeartPrinter has two superior bases: the anterior suction base which is positioned anteriorly on the epicardium, and the posterior suction base which is positioned posteriorly. Deployment of both

superior bases at their target regions defines two of the three points of contact required for HeartPrinter to achieve a stable platform on the heart. Compared to the previous designs,[13,24,25] the new design of the superior suction bases features several updates. Firstly, as seen in Fig. 5A, there is now a smooth top profile in the transition from the distal to proximal end of the suction base, enhancing safety of pericardial contact and enabling greater maneuverability in the intrapericardial space with the introducer arm. Moreover, the bottom region of the suction base that is in contact with the heart has a curved profile (Fig. 5A), which strengthens the vacuum seal formed with the epicardium.

As seen in Fig. 5A-5B, the nitinol introducer arm is slotted into the proximal end of the suction base (Fig. 5C), which enables the operator to control the position and orientation of the suction base. Once the suction base is deployed at its target region on the epicardium and suction is activated, the introducer arm can be slid out from the base and removed from the patient by the operator. The Tygon™ suction line (Fig. 5A-5B) also fits into the proximal end of the suction base, fitting over the suction channel luer fitting (Fig. 5C). This luer fitting provides improvements in geometrical matching and maintaining the vacuum seal with the suction line compared to previous designs where the suction line was slotted into a circular fitting.[13,24,25] With the suction line fitted over the luer fitting, the channel then feeds into the suction seal (Fig. 5D) to interface with the surface of the heart. The suction base also features a channel for the cable to pass from the actuator to the injector head, seen in Fig. 5A-5C. As the posterior suction base is shown in Fig. 5, the anterior suction base has the cable channel on the opposite side.

b) Inferior Suction Base

The model of the inferior suction base is shown in Fig. 6, which is positioned on the epicardium near the apex of the heart. Once the inferior suction base is deployed after the superior bases, the three points of contact required for HeartPrinter to achieve a stable platform on the heart are defined. The new design of the inferior base provides flexibility to the HeartPrinter system by not limiting the deployment of the superior bases, along with improvements for compatibility with the introducer mechanism. The first feature is a flap, as seen in Fig. 6A, which fits into the injector head while deploying the inferior suction base near the apex of the heart. This geometrical matching between the injector head and inferior suction

base is used to insert them together and determine the position of the inferior base, which will be described later. Similarly to the superior bases, the Tygon™ suction line and Nitinol introducer arm (Fig. 6A-6B) are slotted into the proximal end of the suction base at their respective attachment points (Fig. 6C).

The second feature added here is the independence of the inferior suction base. Previously, stiff flexure arms, suction lines, or cables from the superior bases were passed through the inferior suction base before exiting the patient.[13,25] However, this forced the inferior base to be greater than double its current size, and made adherence of the inferior base to the epicardium challenging, particularly when the anterior or posterior cables were actuated, which tended to pull the inferior base off the heart. Although included in this prototype, the anterior and posterior cable channels (Fig. 6B) in fact are not utilized. Therefore, no components from the superior bases pass through the inferior base in this design, allowing the inferior base to be deployed and operated in complete independence from the superior bases. Moreover, similarly to the superior bases, the inferior base features a channel for the injector head cable to pass through (Fig. 6C), and a suction seal to interface with the heart (Fig. 6D).

c) Injector Head

The injector head is shown in Fig. 7. The design features three cleats for the cables passing from each of the suction bases, shown in Fig. 7A-7B. During HeartPrinter's deployment, the inferior suction base's flap is slotted into the injector head's slot (Fig. 7C), enabling the inferior base and injector head to be inserted together. Additionally, there is a slot for a 6-degree-of-freedom (DOF) electromagnetic tracking sensor (3D Guidance, Northern Digital Inc., Waterloo, ON, Canada) to be positioned within the injector head (Fig. 7C). The sides of the injector head are also designed to match geometrically with the suction bases in order to determine the positions of the suction bases with the electromagnetic tracking sensor, described later.

ii. Tabletop Setup

The tabletop instrumentation, which is placed alongside the patient during the procedure, is shown in Fig. 2. The setup consists of a motor control hub and three motors which actuate the cables via spools,

three load cells with load cell transmitters, a data acquisition device for measuring the tension in each of the cables, and power supply for the various components. Suction is provided to the suction bases and the dilating suction tool through flexible suction lines using a PowerVac Aspirator suction pump (Precision Medical, Northampton, PA). Cable guides at the edge of the top platform direct the cables from the load cells to the subxiphoid access port (Fig. 3B). The height of the top platform for the tabletop setup is greater than that of the thorax model (Fig. 3B), in order to aid in positioning the suction bases with the introducer mechanism. The tabletop setup is designed to be placed by the patient's right side, with the cable guides closest to the patient.

C. Surgical Workflow

The surgical workflow for HeartPrinter is shown in Fig. 8. The workflow starts with calibration of the 6-DOF electromagnetic tracker that is placed inside the injector head. After this, the introducer mechanism is used to deploy the suction bases and injector head on the epicardium. Once the robot is deployed, the positions of the suction bases are determined with respect to the electromagnetic tracking transmitter using the tracking sensor in the injector head. A preoperative heart model (e.g., from a computed tomography scan) is then registered to the points captured with the tracker. With a fully registered heart model now available to the operator, they can select injection sites. The positioning system will then control the actuators to move the injector head to the injection sites sequentially. Finally, HeartPrinter can be removed from the patient by the operator after turning off all suction. Throughout the procedure, global position feedback is received from the tracker, and feedback for cable tension is obtained from the load cells.

D. Electromagnetic Tracking Sensor Taring

Prior to positioning the suction bases and injector head on the epicardium with the introducer mechanism, the 6-DOF electromagnetic tracking sensor must be tared for orientation measurements. This is done by inserting the tracking sensor into its slot on the injector head and placing the injector head in front of the electromagnetic tracking transmitter's front hemisphere, with the distal end of the injector head oriented along the positive y-axis of the electromagnetic tracking transmitter. In this study, the

injector head is taped flat to a table that is shared with the transmitter. In the future, a taring jig can be developed to align the injector head on a flat surface with the transmitter.

Once the injector head is positioned with respect to the transmitter, the roll, pitch, and yaw angles of the tracking sensor are zeroed, thereby aligning the sensor's orientation in the injector head to the transmitter. This process allows the operator to place the sensor within the injector head at any orientation, and is critical for determining the positions of the suction bases further on in the workflow. With the 6-DOF electromagnetic tracking sensor now tared to the injector head, the sensor should not be removed from or rotated within the injector head for the duration of the procedure.

E. Introducer Mechanism

i. Design Requirements

a) Size and Shape

A subxiphoid approach is used to insert HeartPrinter with the introducer mechanism through an accessory device such as a cannula. Previously, cannulas used had an inner diameter of 20 mm.[13] Once inserted through the cannula, HeartPrinter is directed towards the pericardium near the apex of the heart. For this, the outer dimensions and profile of the introducer mechanism as well as HeartPrinter's components shall allow passage through such accessory devices. As mentioned previously, testing in this study performed on the thorax model is done with a diameter reducer of 20 mm (Fig. 3B).

b) Approach Mechanism

The angle of approach of the first components for the introducer mechanism used to pass through the skin incision should be angled superficially at approximately 20° to the horizontal plane and superiorly to the immediate left of the left shoulder, ensuring the musculophrenic and superior epigastric arteries are avoided.[33,34] Maintaining a superficial angle during initial advancement is critical for averting deeper abdominal components, however should not be too superficial such that there is risk of puncture to the internal mammary artery.[34] Once over the diaphragm, the angle of the introducer mechanism component can be increased to approximately 45° for a posterior approach directed towards the fibrous pericardium.[33]

c) Ease of Use

Once epicardial access is achieved with the introducer mechanism, access should be maintained through the same point of entry on the pericardium and into the pericardial space in order to deploy the suction bases at their target regions. This ensures that the operator does not have to navigate from the skin to the pericardial space each time for the three suction bases, which would increase procedure time as well as pose a greater injury risk to the patient. This process should be consistent and provide the required manipulability and flexibility to reach the suction base target regions anteriorly, posteriorly, and at the apex of the heart.

ii. Primary Components

The following devices are the key components for the introducer mechanism presented.

a) Tuohy Needle

The 18G 6-in. Tuohy needle (Epimed, Dallas, TX, USA) is shown in Fig. 9. Its objective is to form the point of entry through the pericardium and into the pericardial space, while also aiding with navigation towards the pericardium from the skin. The distal end of the needle features a rounded bevel cutting edge, which allows for the needle to be advanced with the bevel pointed upward and away from the cardiac border to decrease the risk of injury. Moreover, a stylet that fits within the Tuohy needle is used to prevent clogging of the needle's lumen during navigation through surrounding anatomy. Use of a Tuohy needle for epicardial access is a common procedure,[33,34] which was a primary factor in its selection.

b) Dilating Suction Tool

The prototype dilating suction tool, which has an outer diameter of 3.4 mm, is shown in Fig. 10. This device has two functions. The first is to pull away the pericardium using suction in order to create separation between the pericardium and epicardium prior to penetration with the Tuohy needle. Suction is passed through the lumen of the device via a suction line passed through the handle, utilizing the same suction line as for the suction bases. A one-way valve at the proximal end ensures that suction is maintained at the distal end, and allows passage of the Tuohy needle. The second function is to dilate the

opening in the pericardium by means of a tapered distal end. While the width of pericardial space cannot typically be established as pericardial fluid is not evenly spread,[35] the dilating suction tool provides 2 mm exposure of the Tuohy needle at the distal end (Fig. 11) to penetrate through the pericardium, which is normally less than 2 mm thick.[36]

c) Steerable Guide Tool

The steerable guide prototype is shown in Fig. 12. This tool is directed over the dilating suction tool through the point of entry on the pericardium, and is used to sequentially guide the superior suction bases to their target regions on the epicardium. The guide consists of a body with a flexible channel that is fitted into a handle at the proximal end. Within the handle lies a steering knob with a cable spool that is connected to a cable, which runs along the length of the channel body and is knotted at the distal end of the channel body. Rotation of the steering knob causes spooling of the cable, which causes deflection of the steerable channel from the straight configuration (Fig. 12A) to the curved configuration (Fig. 12B). The angle lock shaft is then used to fix a set curvature.

When the steerable guide is within the pericardial space, it can be curved and rotated such that the distal end opens up in the direction of the desired suction base target region, either anteriorly or posteriorly. The respective suction base can then be inserted through the steerable guide tool until it exits the distal end, where it will be guided towards its appropriate target region. When the superior suction bases, which are 6 mm wide, are inserted sequentially through the guide, the 5-mm opening prevents their premature exit out of the channel body before reaching the distal end, while also allowing the injector head cable, suction line, and introducer arm for the respective suction base to be freed from the steerable guide tool once the suction base is positioned at its target region. The 5-mm opening also enables the steerable guide tool to be passed over the dilating suction tool.

iii. Mechanism Description

a) Epicardial Access

The workflow for gaining and maintaining epicardial access is shown in Fig. 13. First, the dilating suction tool is inserted through the 20-mm opening (Fig. 13A) with suction disabled. The point of entry

on the skin is typically 2-3 cm below and slightly lateral to the xiphoid process.[33] To aid with navigation through subcutaneous tissue, the Tuohy needle with its stylet can be used through the dilating suction tool. As per the design requirements, the tool is angled at approximately 20° to the coronal plane, and superiorly to the immediate left of the left shoulder.[33,34] After passing over the diaphragm, the angle of the suction tool can be increased to approximately 45° for a posterior approach towards the fibrous pericardium.[33] When in close proximity to the fibrous pericardium, the Tuohy needle with its stylet should be removed from the suction tool if it is used to aid navigation.

Once the suction tool makes contact with the fibrous pericardium (Fig. 13B), suction can be activated to pull the fibrous and parietal pericardial layers away from the visceral pericardial layer, also referred to as the epicardium. The Tuohy needle is then reinserted through the suction tool without its stylet (Fig. 13C). As exposure of the needle tip at the distal end approaches 2 mm, gentle pressure paired with respiratory movement of the heart is generally enough to pass through the parietal pericardial layer.[33] As the needle passes through the pericardial layers, tenting of the parietal layer is occasionally experienced,[33] and as the needle enters the pericardial space, a sensation of "give" will be felt by the operator.[33,34]

After the Tuohy needle has entered the pericardial space, suction is disabled on the dilating suction tool, and the suction tool is pushed distally over the tip of the Tuohy needle. This inserts the suction tool into the pericardial space and dilates the pericardial opening formed by the Tuohy needle (Fig. 13D). In order to maintain epicardial access in the pericardial space, a J-tip guidewire is used. In this study, a 0.014-in. guidewire is utilized (Fig. 13E). The guidewire is inserted through the dilating suction tool and into the pericardial space (Fig. 13F), and the J-curve will maintain access through the pericardial opening. Finally, the steerable guide tool is inserted over the dilating suction tool and guidewire towards the pericardial opening (Fig. 13G), thereby dilating the opening further until the steerable guide tool is in the pericardial space (Fig. 13H).

b) Posterior Suction Base Positioning

With the steerable guide tool in the pericardial space, the posterior suction base is deployed first at its

target region, shown in Fig. 14. From the tabletop setup, the cable for the posterior base is released by its actuator, allowing the posterior base to be pulled towards the subxiphoid access port with the introducer arm. Meanwhile, as seen in Fig. 14A, the inferior suction base, injector head, and anterior suction base are held near the tabletop setup. Within the pericardial space, the guide tool is then rotated to facilitate its steering in the appropriate direction for posterior access, with the 5-mm opening facing towards the patient's left side (Fig. 14B). The posterior base is then inserted through the steerable guide tool (Fig. 14C) until it exits the distal end of the guide tool and slides posteriorly along the epicardium (Fig. 14D). When the posterior suction bases is at its target region, suction is turned on and the introducer arm is removed from the suction base and patient.

c) Anterior Suction Base Positioning

The mechanism for positioning the anterior suction base is shown in Fig. 15. Firstly, the cable for the anterior base is released by its actuator, while the injector head and inferior suction base are held near the tabletop setup (Fig. 15A). Once the anterior suction base reaches the subxiphoid access port, the guide tool is rotated and steered in the appropriate direction for anterior access, with the 5-mm opening facing towards the patient's right side (Fig. 15B). After inserting the anterior suction through the guide tool, the anterior suction base will slide anteriorly along the epicardium towards its target (Fig. 15C). Once the anterior suction base reaches its target, suction is activated and the introducer arm is retracted from the base and patient.

d) Inferior Suction Base and Injector Head Positioning

The inferior suction base and injector head are deployed together near the apex of the heart, as shown in Fig. 16. Firstly, the steerable guide is removed from the pericardial opening, as epicardial access is now maintained by the cables from the superior bases which connect to the injector. As shown in Fig. 16A, the injector head is slotted over the inferior suction base's flap. Then, the cables from the superior bases are pulled by their actuators, which directs the inferior suction base and injector head towards the access port. When in close proximity to the access port, the nitinol introducer arm and suction line can be attached to the inferior base (Fig. 16B). Next, with gradual spooling of the superior-base cables and using them as

guides, along with manipulation of the introducer arm by the operator, the injector head and inferior suction base are directed through the pericardial opening and towards the apex (Fig. 16C). As with the superior bases, the introducer arm is retracted from the inferior base and the patient once the inferior base reaches its target.

F. Suction Base Position Determination

In this study, position determination of the suction bases was performed on a static heart without beating and the thorax. This is the first study analyzing HeartPrinter in three dimensions on a heart model with a pericardial sac and with suction adherence of the suction bases. In the future, this method will be evolved to function on a beating heart, operating through the subxiphoid access port.[37]

i. Inferior Base

The position of the inferior suction base with respect to the electromagnetic tracking transmitter can only be determined when the injector head is slotted over the inferior base's flap, and is determined as follows. Firstly, the offset distance from the electromagnetic tracking sensor origin within the injector head to the point of interest on the inferior suction base was determined from the computer-aided design (CAD) model prior to the operation. This offset distance was defined to align with the coordinate frame of the electromagnetic tracking transmitter, operating in front of the front hemisphere. The point of interest on the inferior suction base is defined as the center point of the suction seal which would contact the surface of the heart. A visualization of the offset distance between the sensor origin and this point of interest is shown in Fig. 17.

Immediately after the inferior base and injector head are deployed on the epicardium with the introducer mechanism, 100 outputs are collected with the electromagnetic tracking sensor of coordinates and Euler angles. By taking the average of these, a rotation matrix can be determined from the average Euler angles, shown in Eq. 1. To align with the application programming interface for the electromagnetic tracking system, a clockwise *xyz* Euler angle convention is used to define the rotation matrix, shown in Eq. (1). The angles about the z, y, and x axes of the sensor are called azimuth (a), elevation (e), and roll (r), respectively.

$$R = R_x(r)R_y(e)R_z(a) \quad (1)$$

$$= \begin{pmatrix} 1 & 0 & 0 \\ 0 & \cos r & \sin r \\ 0 & -\sin r & \cos r \end{pmatrix} \begin{pmatrix} \cos e & 0 & -\sin e \\ 0 & 1 & 0 \\ \sin e & 0 & \cos e \end{pmatrix} \begin{pmatrix} \cos a & \sin a & 0 \\ -\sin a & \cos a & 0 \\ 0 & 0 & 1 \end{pmatrix}$$

Using the average coordinates of the sensor, the offset distance and the rotation matrix, the position of the point of interest on the inferior suction base can be determined with respect to the electromagnetic tracking transmitter, shown in Eq. (2) to Eq. (4) given a 3x3 rotation matrix, *R*, where *R(n,m)* is the element of the n^{th} row and m^{th} column.

$$x_{inferior\_base} = x_{sensor} + x_{offset} \cdot R(1,1) + y_{offset} \cdot R(2,1) + z_{offset} \cdot R(3,1) \quad (2)$$

$$y_{inferior\_base} = y_{sensor} + x_{offset} \cdot R(1,2) + y_{offset} \cdot R(2,2) + z_{offset} \cdot R(3,2) \quad (3)$$

$$z_{inferior\_base} = z_{sensor} + x_{offset} \cdot R(1,3) + y_{offset} \cdot R(2,3) + z_{offset} \cdot R(3,3) \quad (4)$$

ii. Superior Bases

The position of the anterior suction base is determined as follows. An offset distance from the electromagnetic tracking sensor origin within the injector head to the point of interest on the anterior suction base is calculated preoperatively from the CAD model. This offset distance is calculated assuming the injector head is immediately adjacent to the anterior suction base, where the right face of the anterior base is aligned with the left face of the injector head. After determining the position of the inferior suction base, the actuator for the anterior suction base cable is commanded to pull its cable, while the other two actuators can rotate passively in the opposite direction. This causes the injector head to be released out of the inferior suction base flap and pulled towards the injector head cable channel on the anterior suction base.

As the injector head translates towards the anterior suction base, it will travel along the outer bound of the triangular robot workspace. Using the electromagnetic tracking sensor, these *xyz* points and Euler angles are collected for use in the registration phase of the workflow. Moreover, as the injector head approaches the anterior suction base, the tension in the anterior base cable will increase. By defining a

tension threshold for that cable for when the injector head is immediately adjacent to the anterior suction base, spooling of the anterior base cable is stopped once that tension threshold is met. With the injector head and anterior suction base now aligned and positioned adjacent to each other, the position of the point of interest on the anterior suction base is determined in the same manner as for the inferior suction base, using the average coordinates of the sensor, the offset distance, and the rotation matrix.

This process is then repeated for the posterior suction base, by having the injector head translate towards the posterior base, and adding these points and Euler angles along the trajectory to the collection of points for registration. Finally, the injector head is translated back towards the inferior suction base, and these points and angles are also added to the collection for registration. With the collection of registration points, these are then transformed from the electromagnetic tracking sensor origin within the injector head to the injector head point of interest that is in contact with the heart surface, using the same model equations as for the inferior suction base (Eqs. 1-4). The injector head point of interest is defined as the contact point with the heart that is aligned with the *z*-axis of the sensor origin. With this, the positions of all suction bases on the heart surface are now determined, and a collection of points which define the outer bounds of the triangular workspace for HeartPrinter can be used for registration.

G. Registration

In this study, registration of the anatomical heart model constructed preoperatively to the pose of the robot is assumed to be on a static heart without beating and the thorax. As mentioned, this is the first study analyzing HeartPrinter in three dimensions on a heart model with a pericardial sac and with vacuum adherence of the suction bases. In the future, this method will be evolved to function on a beating heart[38] through a subxiphoid access port.

i. Registration Workflow

As seen in Fig. 8, a preoperative heart model is first input to the registration system. In this study, a three-dimensional object file generated from a scan of the rubber heart is used as input. Along with the three-dimensional heart model, the point cloud that defines the outer bounds of the triangular workspace, which is collected during the suction base position determination phase, is also input to the registration

system. With these two inputs, the registration framework functions as follows. Firstly, on a visual display, the operator must approximately align the general area of the operating region on the heart (the epicardium over the left ventricle) to the point cloud of the outer bounds of the triangular workspace. Then global registration is performed to generally align the heart model to the point cloud. In this study, both visual alignment and global registration are done using CloudCompare (v2.13.beta, 2023). After global registration, the alignment is refined by locally registering the globally transformed heart model to the point cloud of the outer bounds of the triangular workspace using the Iterative Closest Point (ICP) algorithm. ICP was selected as it is the most widely used point cloud registration method for its simplicity and performance.[39] However, since a correspondence between point sets is not initially defined, considering the closest point as the corresponding point introduces potential issues with local optima.[39] This is particularly true when the rotation angle between the two point sets is large.[40] Therefore, as mentioned, the operator must first roughly align the two point clouds to minimize these errors. Once the algorithm converges, the positions of the injector head and suction bases can now be visualized on the registered heart model.

H. Experimental Test Procedures

i. Suction Bases - Suction Performance

The new design of the suction bases was assessed for suction ability against the old suction base prototypes.[24] Five trials ($n = 5$) were performed for each of the two anterior bases (Fig. 18A and 18B), and for the new inferior base (Fig. 18C). The old inferior base (Fig. 18D) was not tested as it could not achieve suction on the rubber heart model. As seen in Fig. 18E for the anterior suction base, a cable was knotted at the suction base through the injector head cable channel, and was looped onto the force gauge. A suction line was then attached to the suction base, and the base was positioned on the rubber heart model at its target region without the beating functionality. Once full vacuum adherence of the suction base to the rubber heart was achieved, the cable was gradually pulled with the force gauge in the same direction that the tabletop actuators would pull the cable. The peak force before the suction base dislodged from the heart was extracted, representing the minimum dislodgement force. A two-sample *t*-

test was used to compare the suction ability of the superior suction bases. Results were considered significant if $p < 0.01$.

ii. Suction Bases - Introducer Arm Retraction Forces

The forces required to retract the introducer arm from the suction bases were collected. As described previously, the introducer arm is removed from a suction base once the base has adhered to its target region on the epicardium. Therefore, these forces must be less than the minimum force that causes the suction base to dislodge from the heart, and is critical in assessing the design of the introducer arm slot. As the introducer arm slot is identical in the superior and inferior bases, and the suction dislodge forces for both bases were already collected, the test was only conducted on a superior suction base. A cable was first knotted around the proximal end of the Nitinol introducer arm, and was looped onto the force gauge. The suction base was then fixed in placed on a table with tape, and the introducer arm was inserted into its slot on the suction base. Five trials ($n = 5$) were performed by gradually pulling the cable proximally with the force gauge and recording the force when the introducer arm was retracted from the suction base. Two-sample *t*-tests were used to compare the introducer arm retraction forces to the suction dislodge forces of the new superior and inferior suction base designs. Results were considered significant if $p < 0.01$.

iii. Epicardial Access Performance Testing

a) Tuohy Needle Insertion Forces

Force measurements for insertion of the Tuohy needle through the pericardium using a subxiphoid approach were collected both with and without use of the dilating suction tool. A 3D printed coupling was used to attach the Tuohy needle to the force gauge for measurements. Ten measurements ($n = 10$) without use of the dilating suction tool are collected to simulate a typical epicardial access procedure that only uses a Tuohy needle,[31,32] while ten measurements ($n = 10$) with the suction tool are used as a comparison. Two sample *t*-test was used to compare results with and without the suction tool, and were considered significant if $p < 0.01$.

b) Dilating Suction Tool - Suction & Dilation Performance

The dilating suction tool was first assessed for suction ability on the pericardium. A 3D-printed coupling was used to attach the dilating suction tool to the force gauge for measurements. Through the access port, the suction tool was inserted towards the pericardial sac at an angle mimicking that of the introducer mechanism procedure described previously with the Tuohy needle held inside it. Once full vacuum adherence of the dilating suction tool on the pericardial sac was achieved with the Tuohy needle inside, the dilating suction tool was pulled with the force gauge. Ten trials ($n = 10$) were performed to capture the force required to separate the tool from the pericardial sac.

The dilating suction tool was then assessed for dilation forces through the pericardium. The same 3D-printed coupling was used to attach the dilating suction tool to the force gauge. On the heart model, an 18G needle was used to create perforations on the pericardial sac. The dilating suction tool was then placed on a perforation and inserted through the pericardial sac to dilate the opening. The peak force when the dilating suction tool penetrated the pericardial sac was recorded. Ten perforations on the pericardial sac were created for ten trials ($n = 10$) with the dilating suction tool.

iv. Superior Suction Base Navigation Ability

As navigation of the superior bases within the pericardial space and along the epicardium using the introducer arm is critical for successful positioning of HeartPrinter at the epicardial target regions, navigation ability of the new superior base design was assessed against the previous superior suction base design. As shown in Fig. 19, a test setup was developed using a foam mat and nylon sock. The nylon sock was fitted snugly over the foam mat, with the edges of the mat clamped down to a table. This provided a tight fit of the nylon sock against the foam mat, replicating a worst-case scenario of the pericardial sac pressing down on the epicardium. The new (Fig. 18A) and old (Fig. 18B) designs of the superior suction bases were manipulated by their appropriate introducer arms, and inserted at the point of entry. The suction base was then slid along the mat until the exit point. Three trials ($n = 3$) were performed for each suction base, and visual observations of navigation ability were recorded.

v. Suction Base Positioning Accuracy

Accuracy in positioning of the suction bases at their target regions was assessed using the 6-DOF

electromagnetic tracking sensor. With the electromagnetic tracking transmitter fixed in place adjacent to the thorax, desired position coordinates were defined for each of the targets on the epicardium of the heart model without beating. Then the introducer mechanism was used to position the suction bases posteriorly, anteriorly, and at the apex of the heart with beating. After the suction bases were positioned on the epicardium, beating of the heart was stopped and the electromagnetic tracking sensor was used to determine their actual position. Positional error of the actual suction base position relative to the desired position is reported by the average root mean square error (RMSE) for each of the target regions across the five trials ($n = 5$) performed for this test. In this test, the positive y-axis was oriented towards the patient's left shoulder, the positive z-axis was oriented downwards towards the patient's posterior, and the positive x-axis was derived using a right-handed coordinate frame.

vi. Suction Base Position Determination Accuracy

Accuracy of determining the positions of the suction bases after HeartPrinter is deployed on the epicardium with the introducer mechanism was assessed using two 6-DOF electromagnetic tracking sensors. The first sensor was used to find the true positions of the suction bases on the rubber heart model, specifically the points of interest in contact with the heart. Then, the suction base position determination algorithm was run with the second sensor placed inside the injector head to find the calculated positions of the points of interest. Positional errors of the calculated positions relative to the true positions are reported by average RMSE for each of the suction bases across the five trials ($n = 5$) performed for this test. In this test, the positive y-axis was oriented towards the patient's left shoulder, the positive z-axis was oriented downwards towards the patient's posterior, and the positive x-axis was derived using a right-handed coordinate frame.

vii. Assessment of Registration Alignment Error

Using the five point clouds obtained from the suction base position determination accuracy test, the three-dimensional heart model was registered to each point cloud. The alignment error between the transformed points of the heart model and the corresponding points from the outer bounds point clouds is recorded as average RMSE in the x, y and z axes across the five trials ($n = 5$) performed for this test. The

average fitness for the five trials is also recorded, where fitness is equal to the number of inlier correspondences divided by the total number of points in the respective triangular outer bounds point cloud. The corresponding point from an outer-bounds point cloud that is associated with a point in the transformed heart model is defined as its closest point, and must have a distance below a set threshold. In this test, the positive *y*-axis was oriented towards the patient's left shoulder, the positive *z*-axis was oriented towards the patient's posterior, and the positive *x*-axis was derived using a right-handed coordinate frame.

Results

A. Suction Bases - Suction Performance

The mean force before the superior suction base dislodged from its target region on the heart was 2.6 ± 0.2 N for the new design and 2.2 ± 0.1 N for the old design. The associated p value was 0.003, representing a statistically significant improvement in suction performance of the new superior base design. The mean force before the new inferior base prototype dislodged from the apex of the heart was 1.1 ± 0.1 N. As described previously, the test could not be performed on the old inferior base.

B. Suction Bases - Introducer Arm Retraction Forces

Mean introducer arm retraction forces from a superior suction base are shown in Table 1, along with a comparison to the suction base dislodge forces collected previously. The average introducer arm retraction force was 0.8 ± 0.1 N. The superior and inferior suction base dislodge forces were greater than the introducer arm retraction forces and statistically significant ($p < 0.0001$ and $p < 0.0014$).

C. Tuohy Needle Insertion Forces

The average Tuohy needle insertion force through the pericardial sac on the rubber heart model was 1.2 ± 0.2 N without the dilating suction tool and 1.5 ± 0.2 N with the dilating suction tool. Insertion of the Tuohy needle with the dilating suction tool was only performed once adequate suction was achieved on the pericardium. The difference between the mean forces was statistically significant ($p = 0.007$); however, this was deemed acceptable and will be explained further.

D. Dilating Suction Tool – Suction & Dilation Performance

For the dilating suction tool, the average force before the tool separated from the pericardial sac was 1.8 ± 0.1 N. This was the average pull away force once full suction adherence was achieved by the dilating suction tool with the Tuohy needle inside at an angle on the pericardial sac. With this force being greater than the Tuohy needle insertion forces with the dilating suction tool collected previously, the pericardial sac can therefore be held during needle insertion. The mean force for dilation by the dilating suction tool through perforations on the pericardial sac with the rubber heart model was 5.5 ± 1.4 N.

E. Superior Suction Base Navigation Ability

Navigation ability of the new superior suction base exceeded that of the old superior suction base. When the old superior suction base was inserted at the point of entry, its front edge got caught on the nylon sock, pulling the sock forwards with it as seen in Fig. 20A-20B. On the contrary, the new superior suction was inserted at the point of entry without getting caught on the nylon sock, as shown in Fig. 20C. As the suction bases were slid along the foam mat towards the exit point, the circular suction line fitting of the old superior suction base was repeatedly catching on the nylon sock, shown in Fig. 20D, while the new superior suction base was able to slide smoothly within the enclosed environment, shown in Fig. 20E.

F. Suction Base Positioning Accuracy

Accuracy for positioning the suction bases at their target regions on the epicardium of the rubber heart model is shown in Table 2. Average RMSE in x, y and z was 9.36 mm for the anterior base, 13.51 mm for the posterior base, and 9.96 mm for the inferior base. The largest positional errors were for the posterior base in the x and z directions at 9.44 mm and 9.32 mm, respectively. Positional error was also the greatest in the x-axis for all bases.

G. Suction Base Position Determination Accuracy

Accuracy for determining the positions of the suction bases on the epicardium of the rubber heart model using the position determination algorithm is shown in Table 3. Average RMSE in x, y and z was 3.07 mm for the anterior base, 3.73 mm for the posterior base, and 1.45 mm for the inferior base. Position

determination accuracy error for both superior suction bases was more than double the error for the inferior suction base. Additionally, position determination accuracy error was the greatest in the *x*-axis for all bases.

H. Assessment of Registration Alignment Error

Registration error between the transformed heart model to the point clouds of the outer workspace bounds is shown in Table 4. Average RMSE for the five trials was 1.14 mm in *x*, 1.02 mm in *y* and 0.829 mm in *z*, and the average fitness was 0.103. Registration of the heart model to one of the point cloud trials collected of the outer workspace is also shown visually in Fig. 21.

Discussion

The developments to HeartPrinter's components for adhering to and operating on the epicardium provide greater stability on the heart's surface and compatibility with the introducer mechanism. Given a bottom curved profile for the suction bases and the suction line being fit over a luer fitting instead of a circular fitting, the vacuum seal that forms with the epicardium was strengthened as demonstrated by the increase in mean suction force compared to the previous design. This ensures a stable platform for HeartPrinter to compensate the heartbeat and respiratory motions of the heart, and decreases the risk of complications and increased procedure time. To further strengthen the stability of the suction bases on the surface of the heart, eliminating any tangling of the suction line and cable for each suction base would be valuable in future designs. Currently, if the cable gets tangled around the suction line it can cause removal of the suction line from the base or pulling of the base away from its target region. This can be addressed with a bi-lumen flexible tube that fits into the suction base, with one lumen for suction and the other for the cable.

For compatibility with the introducer mechanism, the force required to retract the introducer arm from the suction bases was less than the suction adherence force, ensuring that the introducer arm can be removed from the bases once they adhere to their target regions on the epicardium. Additionally, navigation ability within the pericardial sac of the superior suction bases with the introducer arm was

improved. By ensuring a smooth top profile in the transition from the distal to proximal end of the suction base, the new suction base design was able to slide much more smoothly in the constrained environment compared to the old suction base. Not only does this enhance the user experience, it also minimizes the potential patient safety risks such as excessive insertion forces and damage to the suction bases. Furthermore, HeartPrinter's tabletop setup was fully modified to ensure functionality with the introducer mechanism and the components it operates.

The redesigned introducer mechanism met the outlined design requirements of size and shape, approach mechanism, and ease of use. HeartPrinter's footprint was significantly reduced to ensure it could be inserted through a 20-mm cannula. This was driven by a reduction greater than 50% in size of the inferior suction base, geometrical matching of the injector head's flap such that the inferior suction base and injector head can be inserted together without an increase in radial width, and removal of components that pass through the inferior base. To satisfy the approach mechanism requirement, the dilating suction tool can be manipulated to avoid puncturing critical anatomy before reaching the fibrous pericardium and navigated with the Tuohy needle with its stylet through subcutaneous tissue. For ease of use, the J-tip guidewire sufficiently maintained access through the pericardial opening, and with the steerable guide tool inserted over it to dilate the opening and maintain its position in the pericardial sac, this process was repeatable for the suction bases. Further reduction in the size of the steerable guide tool in subsequent designs can help to enhance HeartPrinter's minimal invasiveness and the workflow between different components of the introducer mechanism.

The Tuohy needle insertion force with the dilating suction tool was greater than without the tool; however, this was deemed acceptable, because suction from the dilating tool causes the pericardium to be pulled up against the Tuohy needle, which acts as a free-standing and moveable thin base to puncture against. Therefore, this thin base for puncturing required greater manipulation of the Tuohy needle to puncture through and with it a greater amount of force, whereas without the suction tool the pericardial sac is held stationary against the epicardium. While the suction tool was successful in pulling the pericardium away from the epicardium to minimize the risk of puncture to the epicardium, full suction

ability of the dilating suction tool was not transferred during puncture. This was likely due to leakage at the proximal end out of the valve with movement of the Tuohy needle, as well as contaminants on the pericardial sac that clogged the dilating suction tool. Stability of the puncture site and reduction of suction loss can be improved upon in future designs by using a suction pump with greater vacuum pressure output, as well as increasing the internal diameter of the dilating suction tool to increase the gap around the Tuohy needle, thereby increasing the cross-sectional area for contact. The taper should, however, be maintained at the distal end to ensure a smooth insertion during dilation and minimize the risk of excessive force, as demonstrated in this study with dilation forces through perforations on the pericardial sac.

Successful positioning of the suction bases at the target regions with the introducer mechanism was also demonstrated. Since the target regions are used as general references rather than for high-accuracy absolute positioning, approximately 1 cm of positioning error for each of the bases was sufficient for HeartPrinter to establish its workspace. The posterior base's positional error was the greatest of the three bases due to a larger error in the *z*-axis. This was because of movement of the heart model due to the guide tool and the introducer arm pushing downwards on the heart while positioning the posterior base, and since the bottom half of the heart has to be freely suspended and not supported by the fixture. In future studies, fixturing can be improved to try and minimize deflection of the heart's portion which has to be freely suspended; however, it is also an inherent compliance property of the rubber heart that cannot be fully resolved. Deflection of the heart will however not be a problem *in vivo*. Positional errors were the greatest in the *x*-axis due to the introducer arm pushing the heart forward slightly towards the head within the fixture, as well as a lack of visualization of the suction bases during positioning as only the subxiphoid access port can be seen. In a clinical procedure, this would be addressed with fluoroscopy and the suction bases being radiopaque such that the operator can correct for positioning errors based on the target defined in a planar view.

The suction base position determination algorithm and registration framework represent the first such workflows for HeartPrinter on a heart model with a pericardial sac and vacuum adherence of the suction

bases, and in using an electromagnetic tracking sensor. For the suction base position determination algorithm, the injector head was able to move to each of the suction bases under the pericardial sac. Not only did this output an accurate estimate for the positions of the suction bases and therefore the outer bounds of HeartPrinter's workspace, but also provided the collection of points needed for registration. While the error in determining the positions of the superior suction bases was more than double the error for the inferior base, this could be due to two primary causes. Firstly, the position of the inferior base is collected immediately after positioning on the epicardium without any movement of the injector head. Therefore, there is no movement of the heart within its fixture and no significant movement of the inferior base. Secondly, when the injector head is translated to the superior bases there are high tensions in the cables that pull the injector head. When the injector head makes contact with the superior suction base, there is slight movement of the suction base caused by a combination of this contact force, high cable tension, and slight movement of the heart within its fixture. In future work, the tension threshold and injector head movement rate can be further tuned to reduce the superior suction bases position determination error.

The registration framework provided an effective procedure for aligning the heart model to the point clouds that defined the outer bounds of HeartPrinter's triangular workspace with an average error less than 2 mm. Use of CloudCompare for global registration mimicked how the operator would generally align the heart model on a display, and ICP enabled further registration refinement. As desired and shown in Fig. 21, a good portion of the left side of the heart is defined by HeartPrinter's triangular workspace allowing the operator to select specific injection sites within there. The confidence levels of the triangular workspace point clouds can be increased in the future by having the injector head go to each suction base more than once, thereby densifying the point cloud and allowing for noise to be eliminated, and increasing the registration fitness.

Ensuing design improvements and integration for HeartPrinter will focus on implementing the injection system and heartbeat compensation in a three-dimensional environment, which will require space-time localization and registration. Not only will this permit assessment with improved

representation of the heart and cardiothoracic environment, but will provide further validation to the designs and workflows presented in this study.

Conclusion

This study demonstrates significant design developments to HeartPrinter across its hardware and software infrastructure. This includes the components for adhering to and operating on the epicardium and their compatibility with the introducer mechanism, refinement of the introducer mechanism for positioning the robot on the epicardium with instruments that compliment each other and the tabletop setup, and preliminary workspace determination and registration workflows on a heart model with a pericardial sac and vacuum adherence of the robot's suction bases. With set design requirements that dictated the robot and introducer mechanism's functionality, HeartPrinter can be positioned on the epicardium safely and repeatably, and stably adhere to the beating heart. Moreover, utilization of the electromagnetic tracking sensor in the injector head enabled intraoperative determination of HeartPrinter's workspace and registration of a preoperative three-dimensional heart model.

References

1. Cannatà A, Ali H, Sinagra G, Giacca M. Gene therapy for the heart lessons learned and future perspectives. *Circulation Research*. 2020;126(10):1394-1414. doi:10.1161/CIRCRESAHA.120.315855
2. Ylä-Herttuala S, Baker AH. Cardiovascular gene therapy: past, present, and future. *Molecular Therapy*. 2017;25(5):1095-1106. doi:10.1016/j.ymthe.2017.03.027
3. Ishikawa K, Tilemann L, Fish K, Hajjar RJ. Gene delivery methods in cardiac gene therapy. *The Journal of Gene Medicine*. 2011;13(10):566-572. doi:10.1002/jgm.1609
4. Katz MG, Fargnoli AS, Pritchette LA, Bridges CR. Gene delivery technologies for cardiac applications. *Gene Therapy*. 2012;19(6):659-669. doi:10.1038/gt.2012.11
5. Gonçalves GAR, Paiva RMA. Gene therapy: advances, challenges and perspectives. *Einstein (Sao Paulo)*. 2017;15(3):369-375. doi:10.1590/S1679-45082017RB4024
6. Ishikawa K, Weber T, Hajjar RJ. Human cardiac gene therapy. *Circulation Research*. 2018;123(5):601-613. doi:10.1161/CIRCRESAHA.118.311587
7. Naso MF, Tomkowicz B, Perry WL, Strohl WR. Adeno-associated virus (AAV) as a vector for gene therapy. *BioDrugs*. 2017;31(4):317-334. doi:10.1007/s40259-017-0234-5
8. Ravindran D, Kok C, Farraha M, et al. Gene and cell therapy for cardiac arrhythmias. *Clinical Therapeutics*. 2020;42(10):1911-1922. doi:10.1016/j.clinthera.2020.09.001
9. Fromes Y, Salmon A, Wang X, et al. Gene delivery to the myocardium by intrapericardial injection. *Gene Therapy*. 1999;6(4):683-688. doi:10.1038/sj.gt.3300853
10. Donahue JK. Cardiac gene therapy: a call for basic methods development. *Lancet*. 2016;387(10024):1137-1139. doi:10.1016/S0140-6736(16)00149-5
11. Trivedi A, Hoffman J, Arora R. Gene therapy for atrial fibrillation - how close to clinical implementation? *International Journal of Cardiology*. 2019;296:177-183. doi:10.1016/j.ijcard.2019.07.057
12. Cleveland JC Jr, Shroyer AL, Chen AY, Peterson E, Grover FL. Off-pump coronary artery bypass grafting decreases risk-adjusted mortality and morbidity. *Annals of Thoracic Surgery*. 2001;72(4):1282-1289. doi:10.1016/S0003-4975(01)03006-5
13. Costanza AD, Wood NA, Passineau MJ, et al. A parallel wire robot for epicardial interventions. *Annual International Conference of the IEEE Engineering in Medicine and Biology Society*. 2014:6155-6158. doi:10.1109/EMBC.2014.6945034
14. Mack MJ. Minimally invasive and robotic surgery. *JAMA*. 2001;285(5):568-572. doi:10.1001/jama.285.5.568
15. Beasley RA. Medical robots: current systems and research directions. *Journal of Robotics*. 2012;2012:e401613. doi:10.1155/2012/401613
16. Breault MS, Costanza AD, Wood NA, Passineau MJ, Riviere CN. Toward hybrid force/position control for the Cerberus epicardial robot. *Annual International Conference of the IEEE Engineering in Medicine and Biology Society*. 2015;2015:7776-7779. doi:10.1109/EMBC.2015.7320195
17. Liu C, Moreira P, Zemiti N, Poignet P. 3D force control for robotic-assisted beating heart surgery based on viscoelastic tissue model. *Annual International Conference of the IEEE Engineering in Medicine and Biology Society*. 2011:7054-7058. doi:10.1109/IEMBS.2011.6091783
18. Peters BS, Armijo PR, Krause C, Choudhury SA, Oleynikov D. Review of emerging surgical robotic technology. *Surgical Endoscopy*. 2018;32(4):1636-1655. doi:10.1007/s00464-018-6079-2
19. Harky A, Hussain SMA. Robotic cardiac surgery: the future gold standard or an unnecessary extravagance? *Brazilian Journal of Cardiovascular Surgery*. 2019;34(4):XII-XIII. doi:10.21470/1678-9741-2019-0194
20. Cheng L, Sharifi M, Tavakoli M. Towards robot-assisted anchor deployment in beating-heart mitral valve surgery. *The International Journal of Medical Robotics and Computer Assisted Surgery*. 2018;14(3):e1900. doi:10.1002/rcs.1900
21. Liang F, Yu Y, Wang H, Meng X. Heart motion prediction in robotic-assisted beating heart surgery: a nonlinear fast adaptive approach. *International Journal of Advanced Robotic Systems*. 2013;10(1):82. doi:10.5772/55581
22. Cheng L, Tavakoli M. Switched-impedance control of surgical robots in teleoperated beating-heart surgery. *Journal of Medical Robotics Research*. 2018;03:1841003. doi:10.1142/S2424905X18410039

23. Zhang W, Yao G, Yang B, Zheng W, Liu C. Motion prediction of beating heart using spatio-temporal LSTM. *IEEE Signal Processing Letters*. 2022;29:787-791. doi:10.1109/LSP.2022.3154317
24. Ladak A, Dixit D, Halbreiner MS, Passineau MJ, Murali S, Riviere CN. Introducer design concepts for an epicardial parallel wire robot. *Robotic Surgery: Research and Reviews*. 2021;8:21-38. doi:10.2147/RSRR.S327069
25. Costanza AD, Breault MS, Wood NA, Passineau MJ, Moraca RJ, Riviere CN. Parallel force/position control of an epicardial parallel wire robot. *IEEE Robotics and Automation Letters*. 2016;1(2):1186-1191. doi:10.1109/LRA.2016.2530162
26. Wilde E, Dan S, Wood NA, et al. Parallel position/force control of epicardial wire robot based on ellipsoid geodesy. *International Symposium on Medical Robotics (ISMR)*. 2019:1-6. doi:10.1109/ISMR.2019.8710202
27. Ladak A, Hajjar RJ, Murali S, Michalek JJ, Riviere CN. Cable tension optimization for an epicardial parallel wire robot. *Journal of Medical Devices*. 2023;17(2):021006. doi:10.1115/1.4056866
28. Shi H, Xue T, Yang Y, et al. Microneedle-mediated gene delivery for the treatment of ischemic myocardial disease. *Science Advances*. 2020;6(25):eaaz3621. doi:10.1126/sciadv.aaz3621
29. Qian S, Zi B, Shang WW, Xu QS. A Review on Cable-driven Parallel Robots. *Chinese Journal of Mechanical Engineering*. 2018;31(1):66. doi:10.1186/s10033-018-0267-9
30. Merlet JP. Wire-driven parallel robot: open issues. In: Padois V, Bidaud P, Khatib O, eds. *Romansy 19 – Robot Design, Dynamics and Control*. CISM International Centre for Mechanical Sciences. Springer; 2013:3-10. doi:10.1007/978-3-7091-1379-0_1
31. Gosselin C, Grenier M. On the determination of the force distribution in overconstrained cable-driven parallel mechanisms. *Meccanica*. 2011;46:3-15. doi:10.1007/S11012-010-9369-X
32. Ota T, Patronik NA, Riviere CN, Zenati MA. Percutaneous subxiphoid access to the epicardium using a miniature crawling robotic device. *Innovations*. 2006;1(5):227-231. doi:10.1097/01.IMI.0000240673.14388.fc
33. Romero J, Shivkumar K, Di Biase L, et al. Mastering the art of epicardial access in cardiac electrophysiology. *Heart Rhythm*. 2019;16(11):1738-1749. doi:10.1016/j.hrthm.2019.04.038
34. Romero J, Patel K, Lakkireddy D, et al. Epicardial access complications during electrophysiology procedures. *Journal of Cardiovascular Electrophysiology*. 2021;32(7):1985-1994. doi:10.1111/jce.15101
35. Bogaert J, Francone M. Cardiovascular magnetic resonance in pericardial diseases. *Journal of Cardiovascular Magnetic Resonance*. 2009;11(1):14. doi:10.1186/1532-429X-11-14
36. Ivens EL, Munt BI, Moss RR. Pericardial disease: what the general cardiologist needs to know. *Heart*. 2007;93(8):993-1000. doi:10.1136/hrt.2005.086587
37. Wood NA, Schwartzman D, Passineau MJ, Moraca RJ, Zenati MA, Riviere CN. Organ-mounted robot localization via function approximation. *The International Journal of Medical Robotics and Computer Assisted Surgery*. 2019;15(2):e1971. doi:10.1002/rcs.1971
38. Wood NA, Schwartzman D, Passineau MJ, Moraca RJ, Zenati MA, Riviere CN. Beating-heart registration for organ-mounted robots. *The International Journal of Medical Robotics and Computer Assisted Surgery*. 2018;14(4):e1905. doi:10.1002/rcs.1905
39. Liu H, Zhang Y, Lei L, Xie H, Li Y, Sun S. Hierarchical optimization of 3D point cloud registration. *Sensors*. 2020;20(23):6999. doi:10.3390/s20236999
40. Du S, Xu Y, Wan T, et al. Robust iterative closest point algorithm based on global reference point for rotation invariant registration. *PLoS One*. 2017;12(11):e0188039. doi:10.1371/journal.pone.0188039

FUNDING

This work was partially funded by the U.S. National Institutes of Health (grant nos. R01HL078839 and R01HL105911), and Carnegie Mellon University's GSA/Provost GuSH Grant.

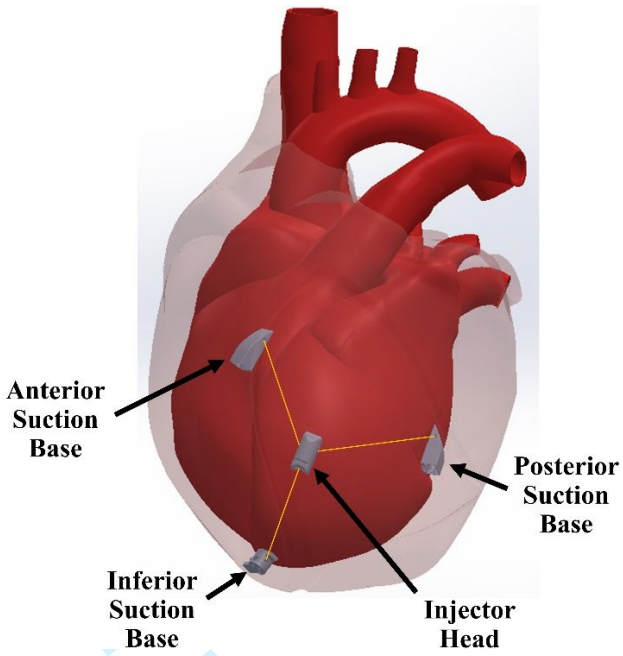

Fig. 1. Depiction of HeartPrinter positioned on the region of the epicardium defined by the left ventricle, under the pericardium. The suction bases, injector head, and cables that connect to the injector head are shown. For simplicity, the suction lines and cables exiting the subxiphoid access port are not shown.

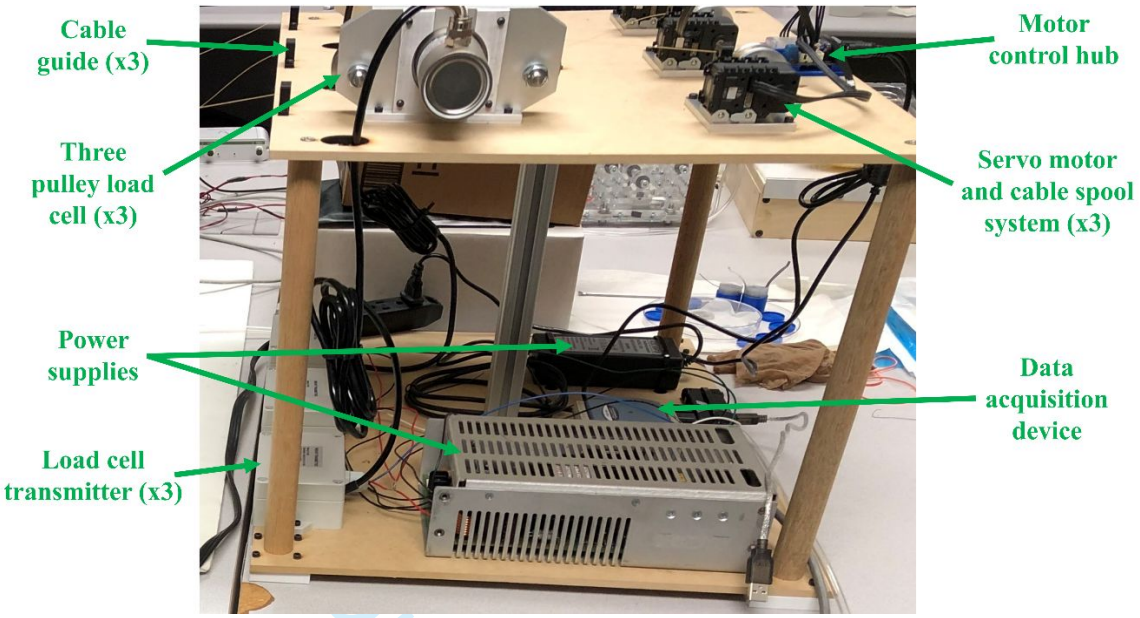

Fig. 2. Tabletop instrumentation for HeartPrinter. The actuators, which control the cable length between the injector head and suction bases are shown. Various other components are shown, such as the load cells and data acquisition device, which are used to measure the tension in each cable.

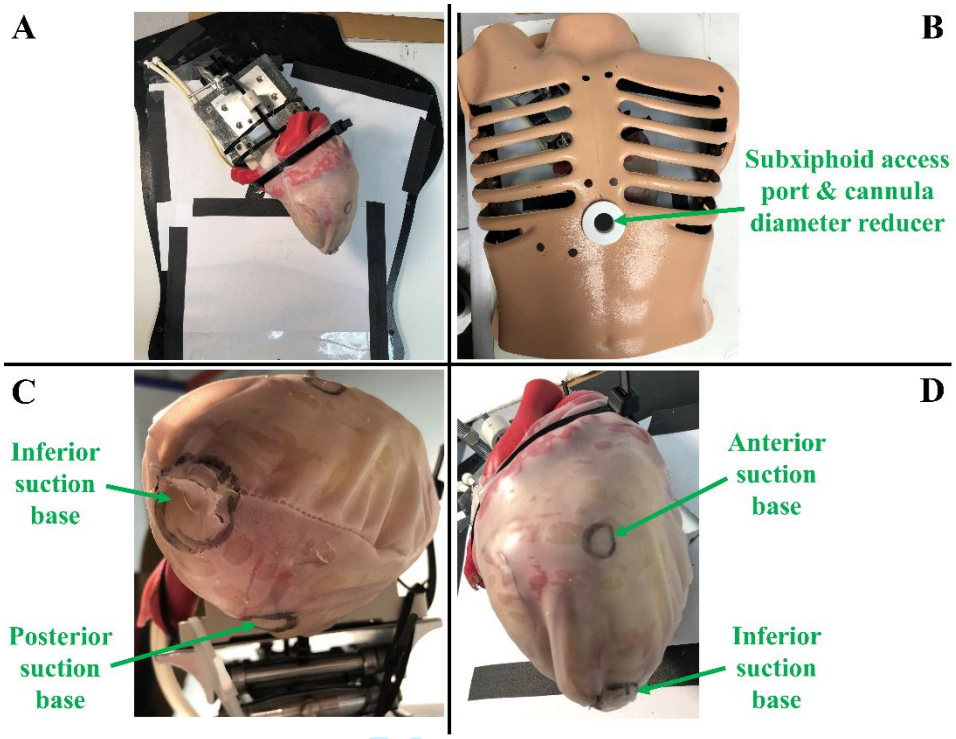

Fig. 3. Testing model setup. **(A)** The rubber heart model mounted to a fixture, and positioned anatomically. The pericardial sac is fitted over the rubber heart. **(B)** The thorax model is shown, with the diameter reducer added to the subxiphoid access port. The target regions for the following suction bases are labelled on the pericardial sac with a marker: **(C)** inferior and posterior suction bases, **(D)** inferior and anterior suction bases.

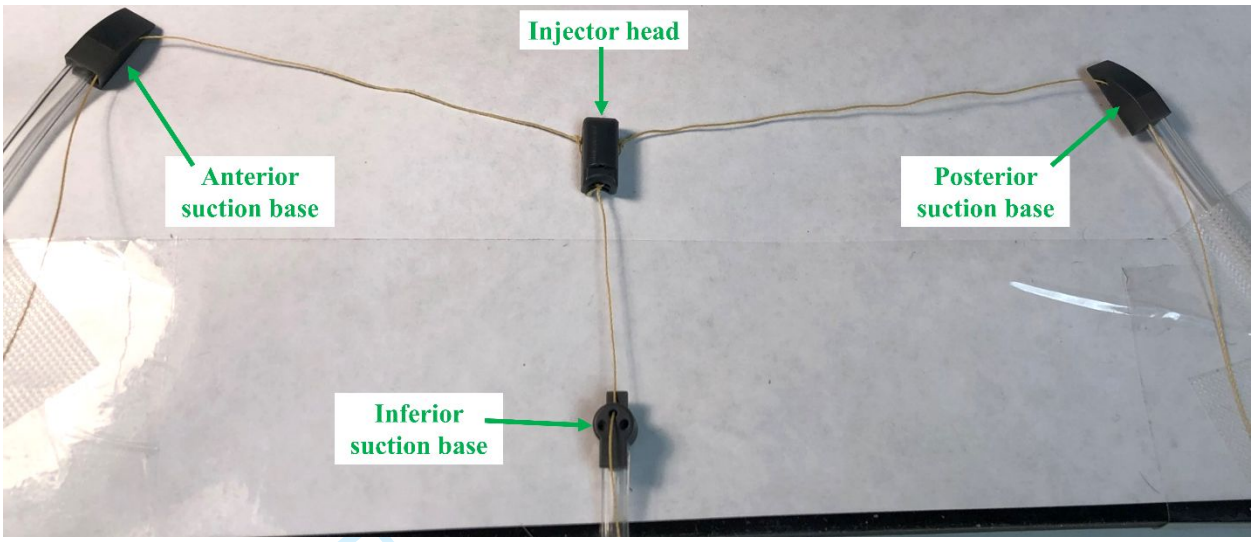

Fig. 4. Prototype of HeartPrinter used in this study. The suction base and injector head are shown along with the suction lines and cables.

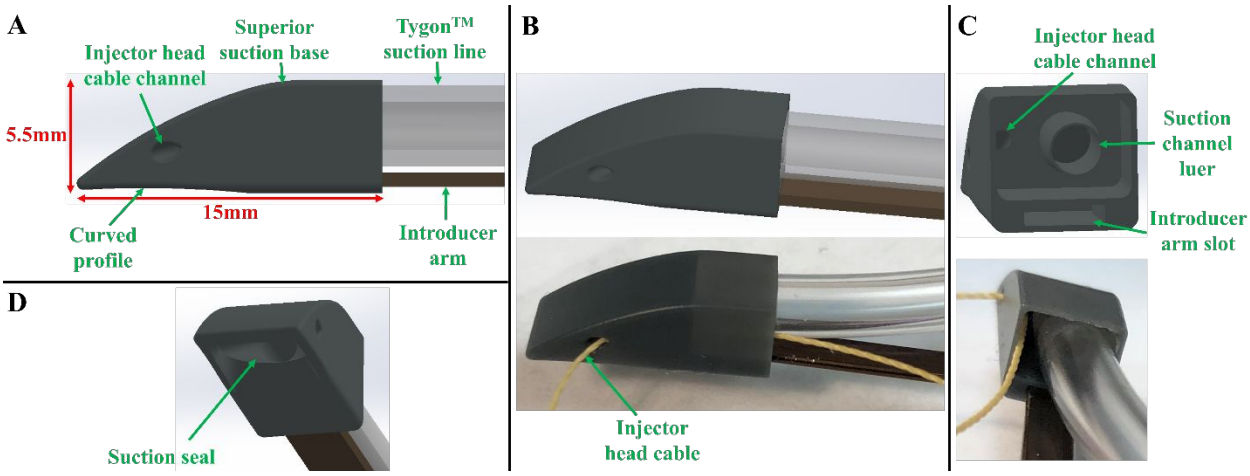

Fig. 5. Design and prototype of the superior suction bases. The posterior suction base is shown. **(A)** Side view of the suction base, which features a curved bottom profile and an injector head cable channel. The Tygon™ suction line and Nitinol introducer arm are slotted into the suction base. **(B)** View of the CAD model and prototyped model for the suction base, suction line, and introducer arm. The injector head cable passing through the cable channel is shown on the prototyped model. **(C)** Second view of the CAD model and prototyped model. The suction line fits over the suction channel luer, the injector head cable passes through the cable channel, and the introducer arm fits into its slot. **(D)** Suction seal which interfaces with the heart's surface to form the vacuum seal.

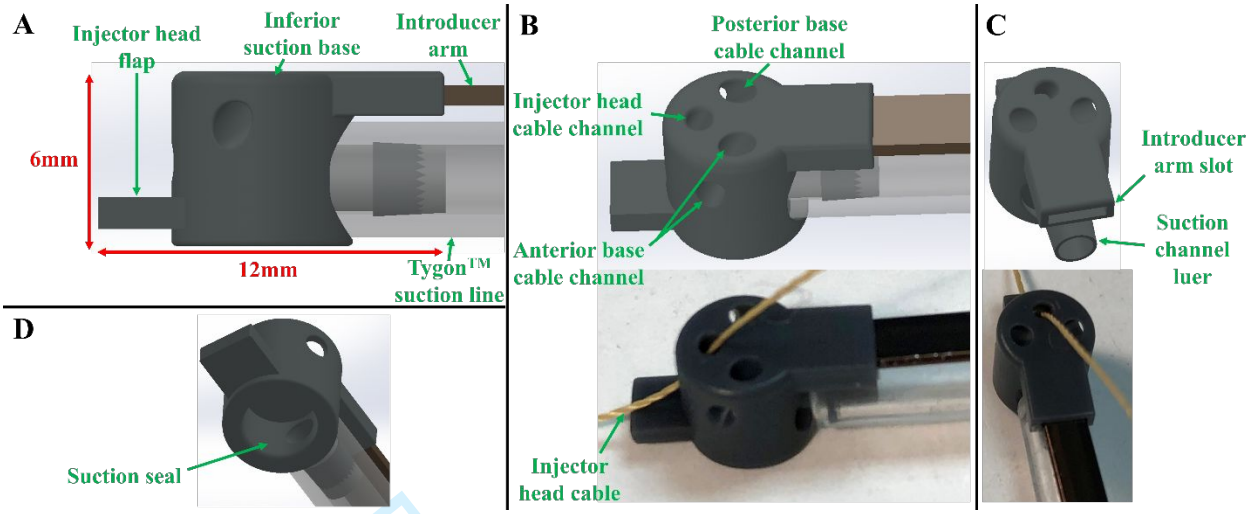

Fig. 6. Design and prototype of the inferior suction base. **(A)** Side view of the suction base, which features a flap for interfacing with the injector head during the insertion process. The Tygon™ suction line and Nitinol introducer arm are slotted into the suction base. **(B)** View of the CAD model and prototyped model for the suction base, suction line, and introducer arm. The injector head cable passing through the injector head cable channel is shown on the prototyped model. There are also two other channels for the cables from the anterior and posterior suction bases, which is a continued feature from previous designs, but are not used in this study. **(C)** Second view of the CAD model and prototyped model. The suction line fits over the suction channel luer, the injector head cable passes through the injector head cable channel, and the introducer arm fits into its slot. **(D)** Suction seal which interfaces with the heart's surface to form the vacuum seal.

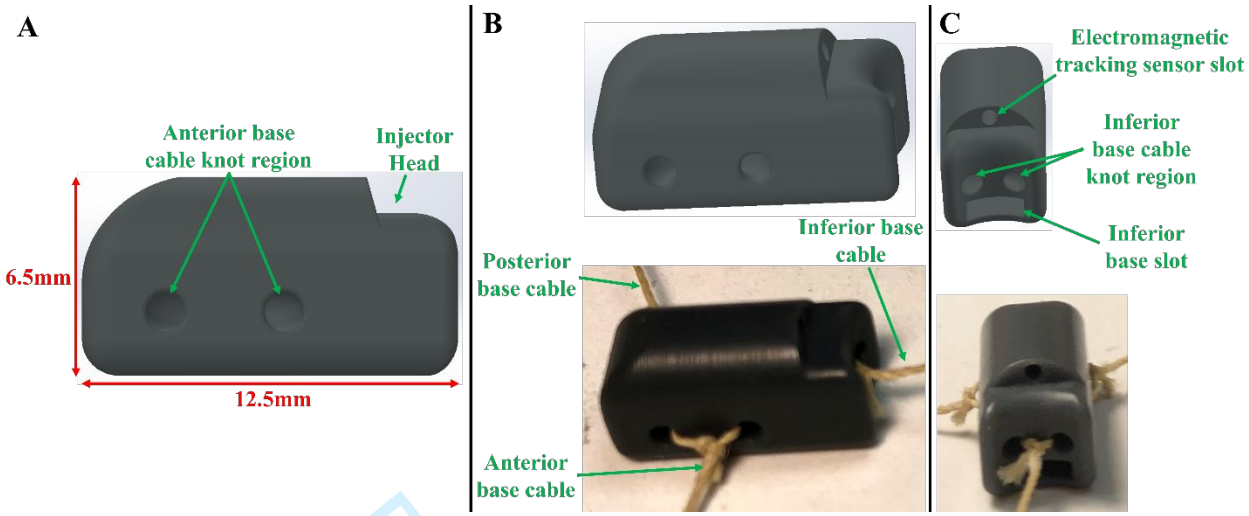

Fig. 7. Design and prototype of the injector head. The injection system is not yet incorporated. **(A)** Side view of the injector head with knot regions for cables from each of the bases. **(B)** View of the CAD model and prototyped model for the injector head. The cables from each of bases are attached to the injector head. **(C)** Second view of the CAD model and prototyped model. Slots for a 6-DOF electromagnetic tracking sensor and the inferior base flap are shown, as well as the inferior base cable knot region.

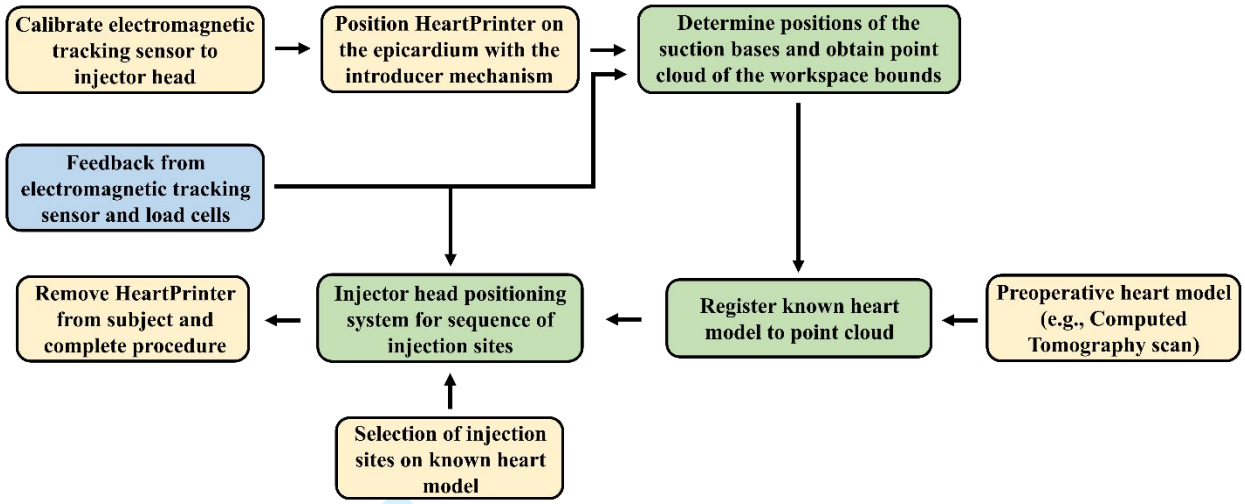

Fig. 8. Surgical workflow for HeartPrinter. Processes in green are primarily system controlled, and processes in yellow are primarily operator controlled. The system begins by calibrating the electromagnetic tracking sensor placed inside the injector head, followed by positioning the robot on the epicardium with the introducer mechanism. This is followed by determination of HeartPrinter's workspace, registration, and positioning of the injector head at various injection sites. Throughout the procedure, global position feedback is received from the electromagnetic tracking sensor, and feedback for tension in the cables is received from the load cells.

Fig. 9. 18G by 6 in. Tuohy needle. The needle features a rounded bevel cutting edge at the distal end. This allows for the needle to be advanced with the bevel pointed upward and away from the cardiac border to decrease the risk of injury. The needle also comes with a stylet which prevents clogging of the needle's lumen while navigating the needle through surrounding anatomy when approaching the pericardium.

Fig. 10. Prototype of the dilating suction tool. The device provides suction ability through its lumen which allows the pericardium to be pulled away from the epicardium prior to penetrating through the pericardium with the Tuohy needle. The distal end is tapered to dilate the point of entry through the pericardium. A one-way valve at the proximal end ensures that suction can be maintained at the distal end, and allows passage of complimentary devices, specifically the Tuohy needle.

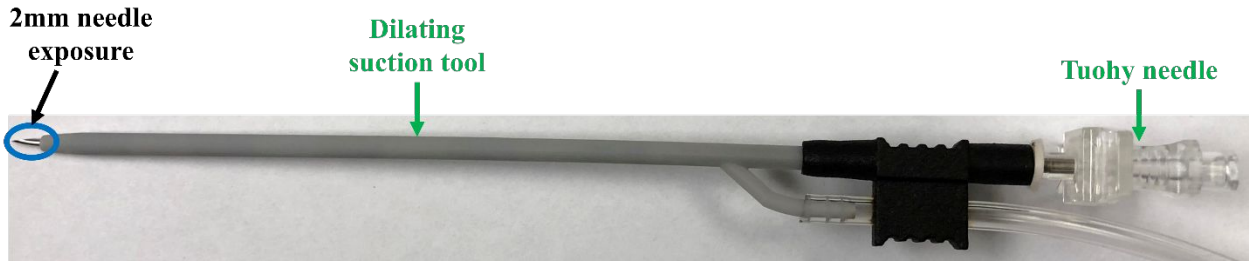

Fig. 11. Passage of the Tuohy needle through the dilating suction tool. The Tuohy needle is inserted at the proximal end of the dilating suction tool, through the one-way valve. The Tuohy needle can be inserted until 2 mm exposure of the needle tip is achieved at the distal end, which occurs when the Tuohy needle handle makes contact with the proximal end of the dilating suction tool.

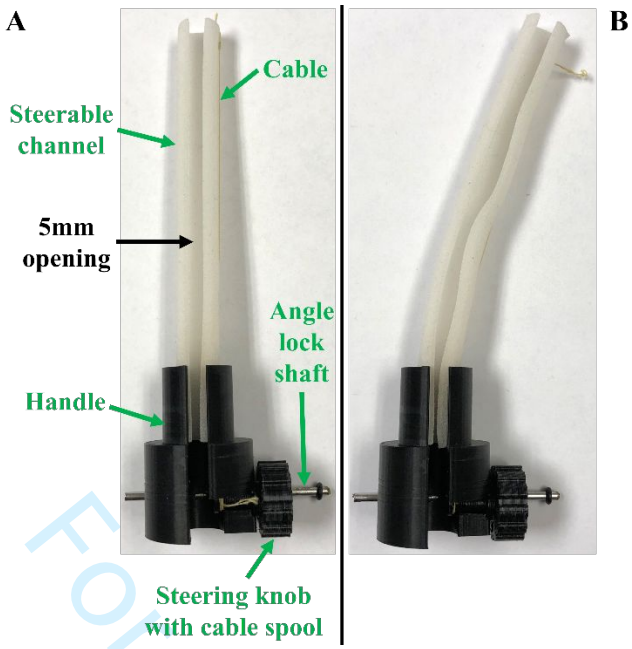

Fig. 12. Prototype of the steerable guide tool shown in the **(A)** straight configuration, and **(B)** curved configuration. The device features a flexible channel body fitted into a handle, with a cable passing along the length of the channel body. The cable is knotted at the distal end of the channel body, and is wrapped around a cable spool placed within the handle at the proximal end. Rotation of the steering knob causes spooling of the cable, thereby causing deflection of the steerable channel. The angle lock shaft is used to fix the steerable guide tool to a set a curvature. The 5 mm opening prevents premature exit of the suction bases and injector head, which are 6 mm wide, and allows the steerable guide tool to be passed over the dilating suction tool.

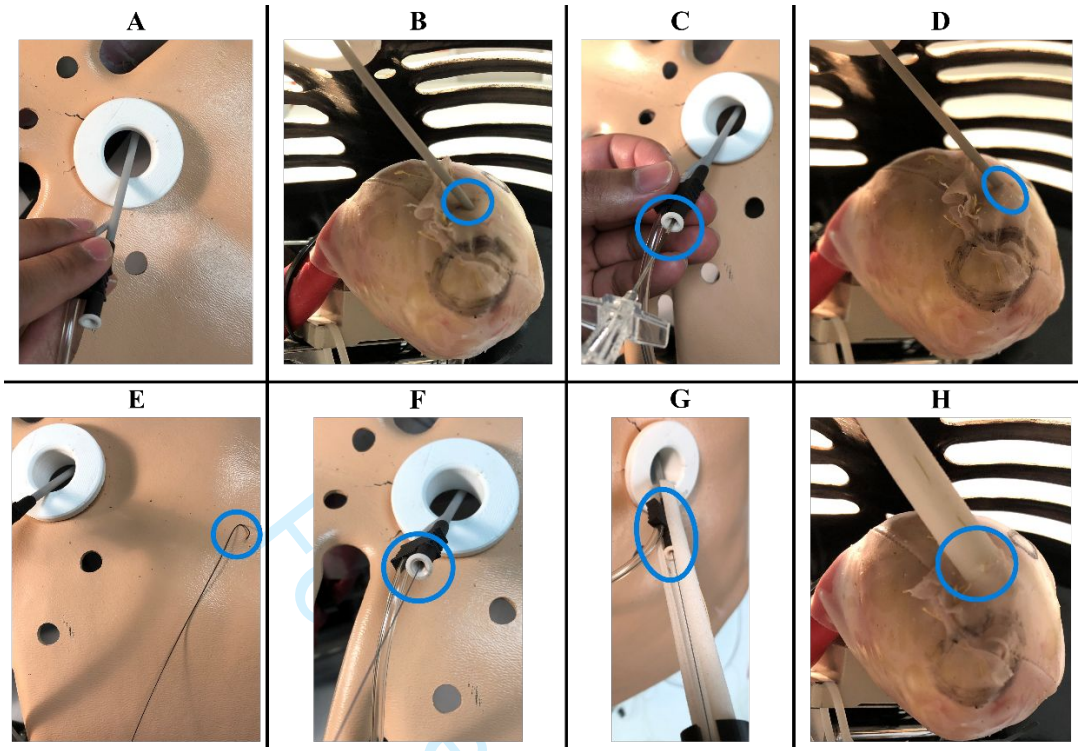

Fig. 13. Workflow for gaining and maintaining epicardial access with the introducer mechanism. **(A)** The dilating suction tool is inserted through the 20 mm opening, and targeted towards the pericardium near the apex of the heart. The Tuohy needle with its stylet can be used with the dilating suction tool to facilitate navigation through surrounding anatomy. **(B)** The dilating suction tool contacts the pericardium near the apex of the heart. Suction is then activated to pull the pericardium away from the epicardium. **(C)** The Tuohy needle is inserted through the dilating suction tool in order to penetrate the pericardium, which is achieved with gentle pressure coupled with respiratory movement of the heart. **(D)** The dilating suction tool is pushed distally over the tip of the Tuohy needle in order to enter and dilate the pericardial opening, and the Tuohy needle is removed. The dilating suction tool is now in the pericardial space. **(E)** A J-tip guidewire is used to maintain epicardial access. **(F)** The J-tip guidewire is inserted through the dilating suction tool and into the pericardial space. **(G)** The steerable guide tool is inserted over the dilating suction tool towards the pericardial opening. **(H)** The steerable guide tool is in the pericardial space.

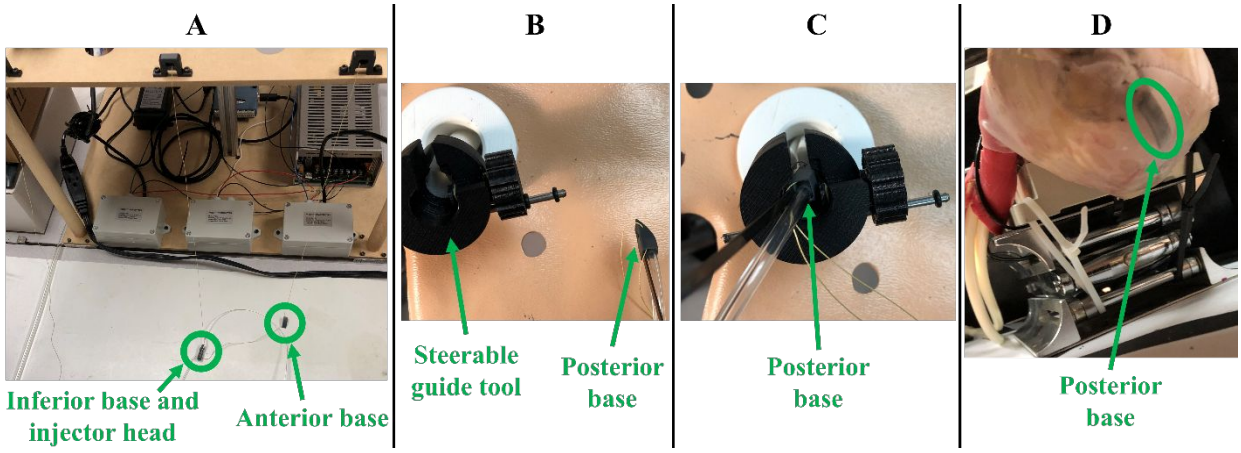

Fig. 14. Workflow for positioning the posterior suction base at its target region on the epicardium. **(A)** The cable for the posterior base is released by its actuator, allowing the posterior base to be pulled towards the patient. The inferior base, injector head, and anterior base are held near the tabletop setup. **(B)** After the steerable guide tool is rotated and steered in the appropriate direction for posterior access, the posterior base is oriented for insertion through the steerable guide tool. **(C)** The posterior base is inserted through the steerable guide tool. **(D)** The posterior base sliding posteriorly along the epicardium is shown after exiting the distal end of the steerable guide tool.

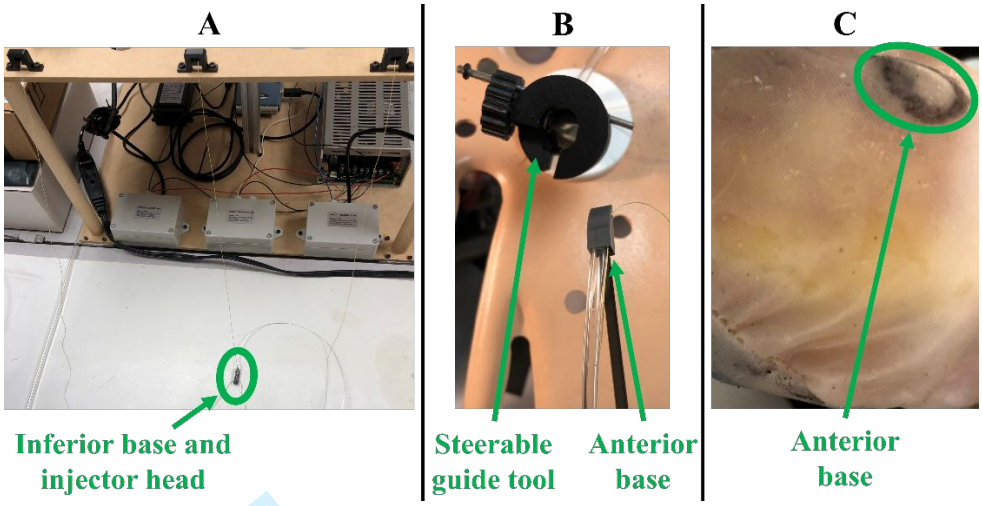

Fig. 15. Workflow for positioning the anterior suction base at its target region on the epicardium. **(A)** The cable for the posterior base is released by its actuator, allowing the anterior base to be pulled towards the patient. The inferior base and injector head are held near the tabletop setup. **(B)** After the steerable guide tool is rotated and steered in the appropriate direction for anterior access, the anterior base can be inserted through the steerable guide tool. **(C)** The anterior base sliding anteriorly along the epicardium is shown after exiting the distal end of the steerable guide tool.

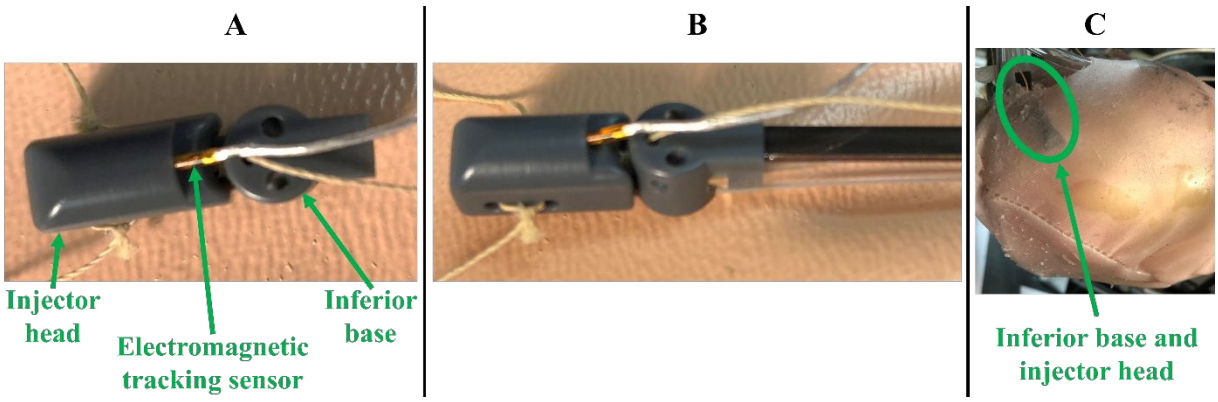

Fig. 16. Workflow for positioning the inferior suction base and injector head near the apex of the heart. **(A)** To position the inferior suction base and injector head together, the injector head is slotted over the inferior base's flap. **(B)** The cables from the superior bases are pulled with their actuators to direct the inferior suction base and injector head towards the subxiphoid access port. Once in close proximity to the access port, the introducer arm and suction line are attached to the inferior base. **(C)** Using the cables of the superior bases as guides and with their gradual spooling, the injector head and inferior base are directed towards the pericardial opening for positioning at the apex.

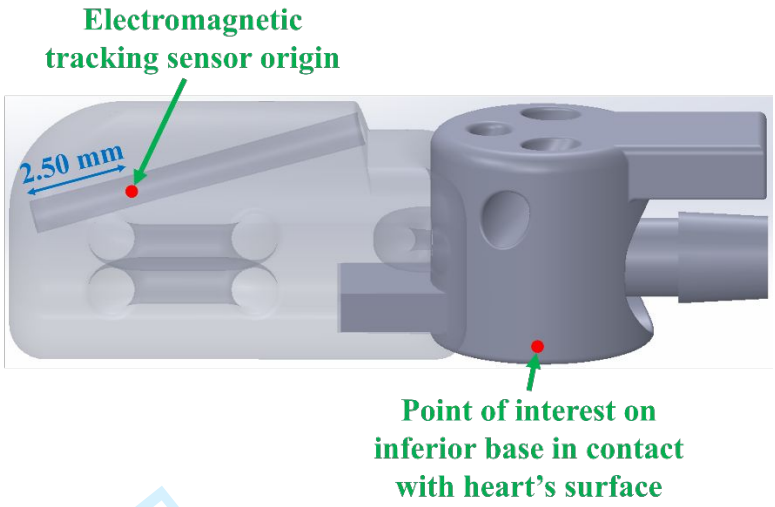

Fig. 17. Visualization of the offset distance from the electromagnetic tracking sensor origin within the injector head to the point of interest on the inferior suction base that is in contact with the heart's surface.

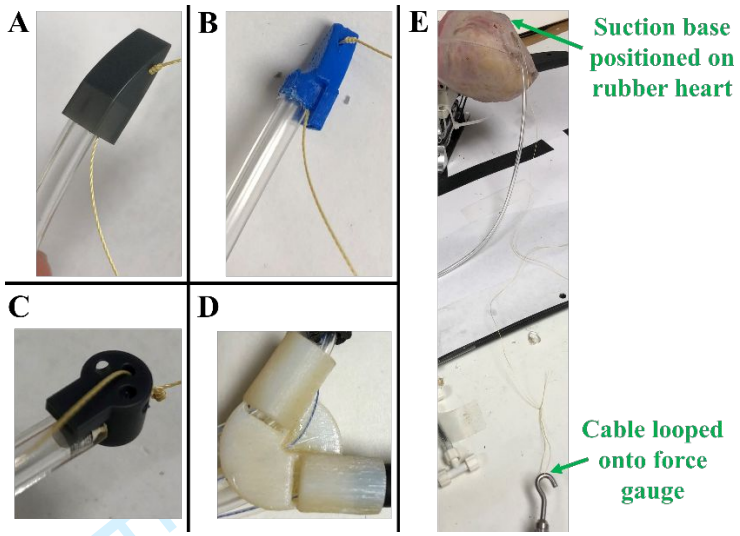

Fig. 18. Set-up for suction performance testing for the suction bases. A cable is knotted through the injector head cable channel and a suction line is attached to the: **(A)** new anterior base, **(B)** old anterior base, and **(C)** new inferior base. **(D)** Old inferior base prototype, which could not achieve suction on the rubber heart model and was not tested. **(E)** Anterior suction base positioned at its target region on the rubber heart model without the beating functionality. The cable was looped onto the force gauge and pulled to record the force before dislodging of the suction base. Testing of the new inferior suction base was done with it positioned at the apex of the heart.

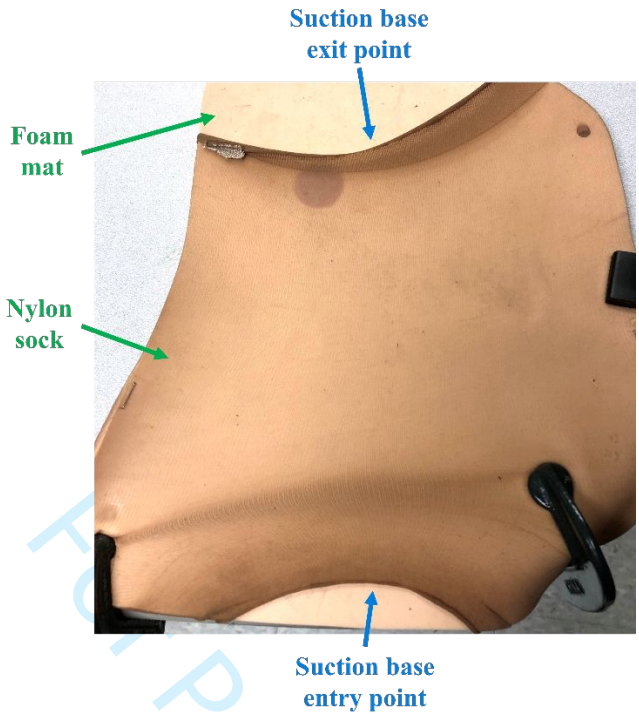

Fig. 19. Test setup to evaluate navigation ability of the superior suction bases in the pericardial space. A nylon sock is fitted snugly over a foam mat, with the edges of the mat clamped down to a table. This provides a snug fit of the nylon sock pressing down on the foam mat, mimicking a worst case scenario of the pericardial sac pressing down on the epicardium. The old and new designs of the superior suction bases were manipulated by their appropriate introducer arms, and inserted at the entry point. The suction base was slid along the mat until reaching the exit point.

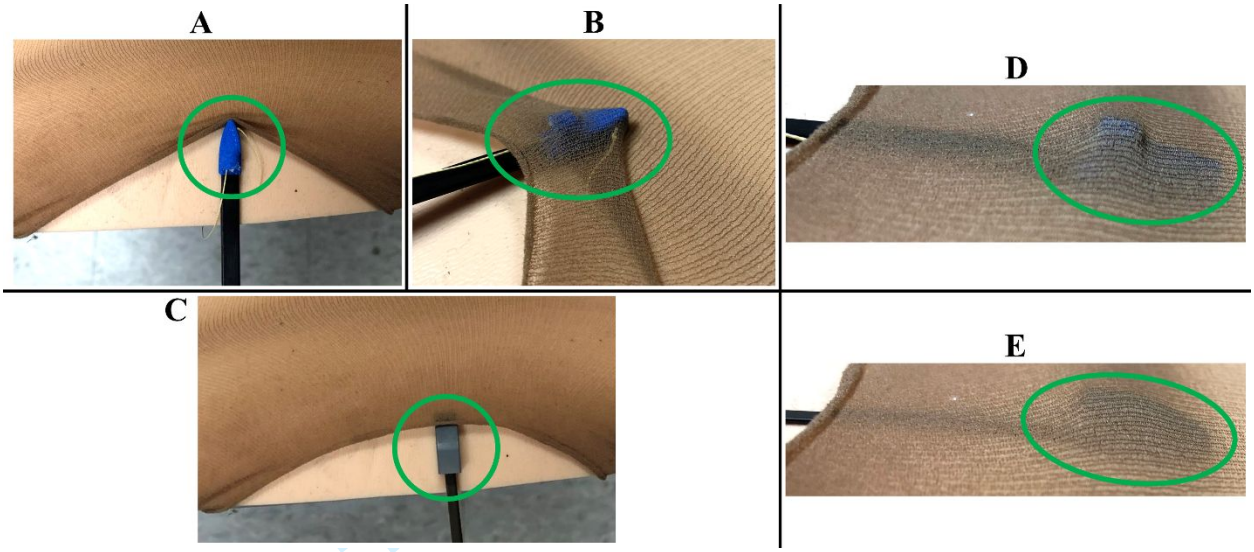

Fig. 20. Navigation ability assessment of the old and new superior suction base designs in the nylon sock setup. **(A)** Insertion of the old superior suction base at the point of entry. **(B)** Front edge of the old superior suction base caught on the nylon sock. **(C)** Insertion of the new superior suction base at the point of entry. Guidance of the old superior suction base along the foam mat and towards the exit point for the **(D)** old superior suction base, and **(E)** new superior suction base.

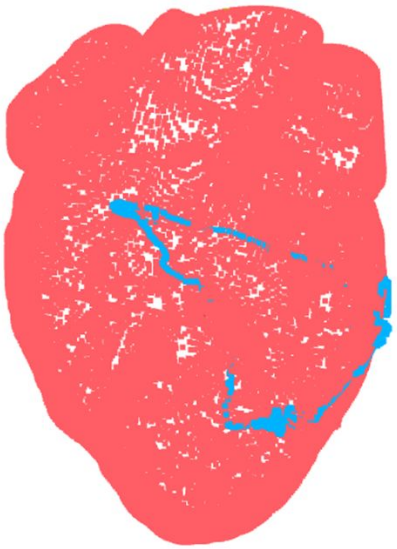

Fig. 21. Registration visualization of the heart model to one of the point cloud trials collected of the outer workspace at the left side of the heart.

Table 1. Suction base dislodge forces from the rubber heart as a measure of suction strength for the new designs compared to the introducer arm retraction forces

Suction Base Type	Suction Base Dislodge Force [Mean ± SD]	Introducer Arm Retraction Force [Mean ± SD]	*p* value
Superior	2.6 ± 0.2	0.8 ± 0.1	< 0.0001
Inferior	1.1 ± 0.1		0.0014

Table 2. Average accuracy for positioning the suction bases at their target regions on the epicardium of the rubber heart model without beating

Suction Base	***n***	**Average RMSE**			
		***x* [mm]**	***y* [mm]**	***z* [mm]**	**Total [mm]**
Anterior	5	6.53	4.56	4.92	9.36
Posterior		9.44	2.56	9.32	13.51
Inferior		7.11	4.91	4.95	9.96

Table 3. Average accuracy for determining the positions of the suctions bases on the epicardium of the rubber heart model without beating using the position determination algorithm

Suction Base	***n***	**Average RMSE**			
		***x* [mm]**	***y* [mm]**	***z* [mm]**	**Total [mm]**
Anterior	5	2.03	1.20	1.96	3.07
Posterior		2.32	2.22	1.90	3.73
Inferior		1.08	0.732	0.633	1.45

Table 4. Mean registration error between the transformed heart model to the point clouds of the outer workspace bounds

n	**Average Fitness**	**Average RMSE**			
		***x* [mm]**	***y* [mm]**	***z* [mm]**	**Total [mm]**
5	0.103	1.14	1.02	0.829	1.74